Master's Thesis

Analysis of the Cycle Life Characteristics of Lithium-Ion Batteries according to their Anode Density in High Rate Charging

HO YOUNG NA

Department of Energy Engineering

(Battery Science and Technology)

Ulsan National Institute Science and Technology

2021

Analysis of the Cycle Life Characteristics of Lithium-Ion Batteries according to their Anode Density in High Rate Charging

HO YOUNG NA

School of Energy and Chemical Engineering
(Battery Science and Technology)

Ulsan National Institute Science and Technology

Analysis of the Cycle Life Characteristics of Lithium-Ion Batteries according to their Anode Density in High Rate Charging

A thesis/dissertation submitted to
Ulsan National Institute of Science and Technology
in partial fulfillment of the
requirements for the degree of
Master of Science

HO YOUNG NA

12/22/2020

Approved by

Advisor
KYEONG-MIN JEONG

Analysis of the Cycle Life Characteristics of Lithium-Ion Batteries according to their Anode Density in High Rate Charging

HO YOUNG NA

This certifies that the thesis/dissertation of HO YOUNG NA is approved.

12/22/2020

Advisor: KYEONG-MIN JEONG

HYUN-KON SONG

DONG-HWA SEO

Contents

Abstract

Recently, Li-ion batteries have become battery technologies ranging from electric vehicles to grid packing system. Although a lot of automakers are announcing electric forms with its products, range anxiety and the time required to charge the batteries are even now a frequent worry. Extreme fast charging, by aiming 20 minutes recharge time for 80% SOC, is composed to quicken mass market acceptance of electric vehicles currently. However, these goals not only inhibit Li deposition but also require good lifetime for offering a good performance. By changing the electrode density of anode in the whole NCM811/graphite lithium-ion battery, delaying cell degradation were attempted. This work was investigated using several methods such as XRD, XPS and SEM after cycle life test. Also, variations of charging protocol were often made to avoid mechanical stress condition when Li plating is possible by reducing heat generation. In addition, superficial film construction was not even after cycling in high rate charging and 1C discharging. This non-even modification more followed in active material delamination from the current collector because of the changes of charging protocol and electrode density of anode

List of Figures

Figure 25. F 1s XPS spectra of anode (a) 1.5g/cc 5C charging 1C discharging depth profiling 0s (b) 1.5g/cc 3C charging 1C discharging (c) 1.5g/cc 5C charging 1C discharging depth profiling 200s (d) 1.5g/cc 3C charging 1C discharging depth profiling 200s (e) 1.5g/cc 5C charging 1C discharging depth profiling 1000s (f) 1.5g/cc 3C charging 1C discharging depth profiling 1000s

Figure 26. F 1s XPS spectra of anode (a) 1.7g/cc 3C charging 1C discharging depth profiling 0s (b) 1.7g/cc 5C charging 1C discharging (c) 1.7g/cc 3C charging 1C discharging depth profiling 200s (d) 1.7g/cc 5C charging 1C discharging depth profiling 200s (e) 1.7g/cc 3C charging 1C discharging depth profiling 1000s (f) 1.7g/cc 5C charging 1C discharging depth profiling 1000s

Figure 27. O 1s XPS spectra of anode (a) 1.5g/cc 5C charging 1C discharging depth profiling 0s (b) 1.5g/cc 3C charging 1C discharging (c) 1.5g/cc 5C charging 1C discharging depth profiling 200s (d) 1.5g/cc 3C charging 1C discharging depth profiling 200s (e) 1.5g/cc 5C charging 1C discharging depth profiling 1000s (f) 1.5g/cc 3C charging 1C discharging depth profiling 1000s

Figure 28. O 1s XPS spectra of anode (a) 1.7g/cc 3C charging 1C discharging depth profiling 0s (b) 1.7g/cc 5C charging 1C discharging (c) 1.7g/cc 3C charging 1C discharging depth profiling 200s (d) 1.7g/cc 5C charging 1C discharging depth profiling 200s (e) 1.7g/cc 3C charging 1C discharging depth profiling 1000s (f) 1.7g/cc 5C charging 1C discharging depth profiling 1000s

Figure 29. C 1s XPS spectra of anode (a) 1.5g/cc 5C charging 1C discharging depth profiling 0s (b) 1.5g/cc 3C charging 1C discharging (c) 1.5g/cc 5C charging 1C discharging depth profiling 200s (d) 1.5g/cc 3C charging 1C discharging depth profiling 200s (e) 1.5g/cc 5C charging 1C discharging depth profiling 1000s (f) 1.5g/cc 3C charging 1C discharging depth profiling 1000s

Figure 30. C 1s XPS spectra of 1.7g/cc anode (a) 1.7g/cc 3C charging 1C discharging depth profiling 0s (b) 1.7g/cc 5C charging 1C discharging (c) 1.7g/cc 3C charging 1C discharging depth profiling 200s (d) 1.7g/cc 5C charging 1C discharging depth profiling 200s (e) 1.7g/cc 3C charging 1C discharging depth profiling 1000s (f) 1.7g/cc 5C charging 1C discharging depth profiling 1000s

List of Tables

I. Introduction

1.1. Lithium-ion batteries

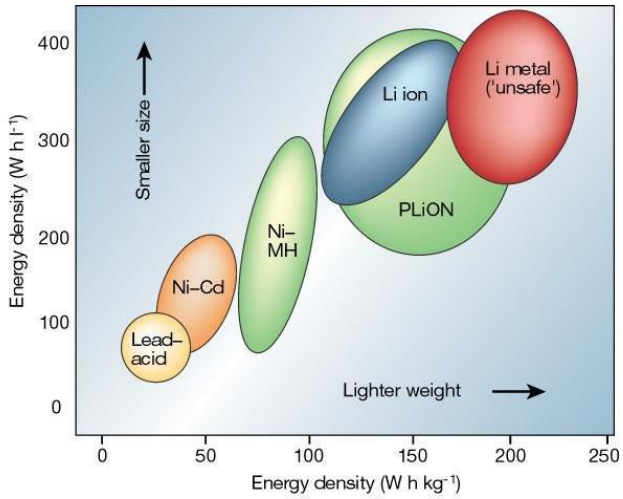

Figure 1. Volumetric and Gravimetric energy density of various sorts of battery science [21]

Recently, Li ion batteries have been remarkably improved and are being adopted as the first option for a variety of electronic device. Lithium-ion batteries are currently used in devices such as laptop, drone, and smart phones. The design of the higher energy density and higher voltage is also used as a power supply, ranging from light electric vehicles like electric bicycles to electric scooters, which are even larger motor vehicles. Figure 1[21] compares the volume and weight energy densities of various battery technologies. Among these technologies, lithium-based batteries outperform others. This is because of the superior energy density and flexible configuration of the Li system.

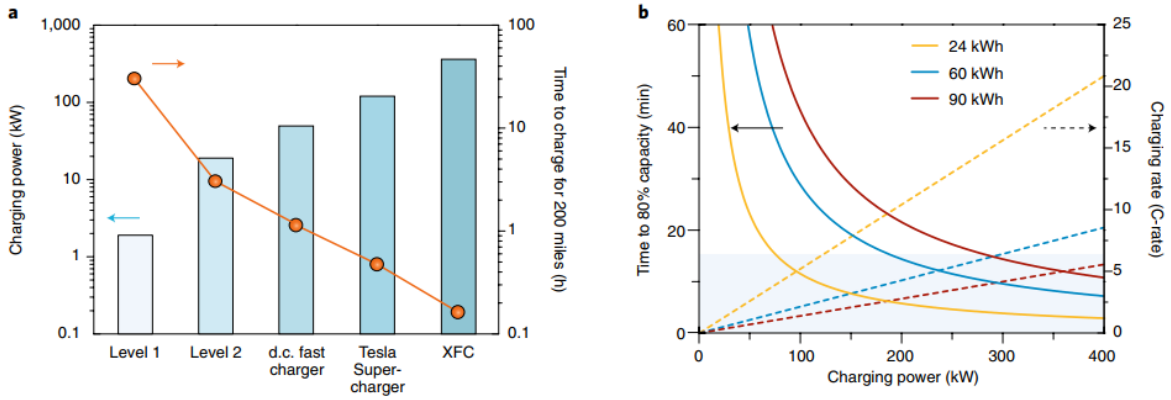

Figure 2. Overview of the technological requests for EV battery rapid charging

Figure 2[1] shows comparison between currently available charging methods and super-fast charging method. Levels 1 and 2 showed the power of charging defined by the Society of Automotive Engineers

standard J1772 and burgeoning direct current fast charger showed a maximum power of 50kW utilized. Tesla Supercharger showed 120 kW maximum power of Supercharging V2 stations. In this graph, the charging power for extreme fast charging were calculated. The automobile energy consumption is supposed to be 285 Wh per mile.[2]

Figure 2b demonstrates a theoretical scheme of charging time and charging rate as a function of charging power. At a certain power, a bigger battery pack needs time for charging longer. Thus, focusing on the chargers based on the pack size essential.

Equation 1. Equation of energy density

Energy density = (Cell voltage) x (Specific capacity) / (Mass loading) / (Thickness)

= (Cell voltage - Overvoltage) x (Specific capacity) / (Mass loading) / (Thickness)

$$Wh/_{L} = V_{cell} \cdot Ah \Big/ kg \cdot \frac{L}{kg}$$

$$= V_{cell} \cdot Ah/_{kg} \times d$$

$$= (V_{cell} - \eta_s - \eta_c - \phi_{IR}) \cdot Ah/_{kg} \times d$$

$$= (V_{cell} - \eta_s - \eta_c - \phi_{IR}) \cdot Ah/_{kg} \times mg/cm^2 \times 1/cm$$

$$= (V_{cell} - \eta_s - \eta_c - \phi_{IR}) \cdot Ah/_{kg} \text{ x Loading level x } 1/_{Thickness}$$

As such, the increasing demand that high-speed charging is important in the EV market. In addition, energy density per volume is a crucial factor in the battery business of the future, especially energy density per volume, an important measure for the electric vehicle market. Through the above Equation 1, the energy density required for an electric vehicle can be met by reducing the overvoltage and reducing the thickness while increasing the cell voltage. Since rechargeable batteries for electric vehicles should have a short charging time, light weight, and excellent performance, competition for technology development is expected to be fierce, focusing on lithium-ion batteries.

1.2 Research about Lithium-Deposition

1.2.1 Hint of Li deposition

When Li deposition occurs on the anode, it greatly contributes to the degradation of the lithium-ion battery. Li deposition is associated with rapid charging capabilities and safety issue, as well as severe life limitations. Lithium deposition in lithium-ion cells is no longer controlled to low temperature operating conditions.

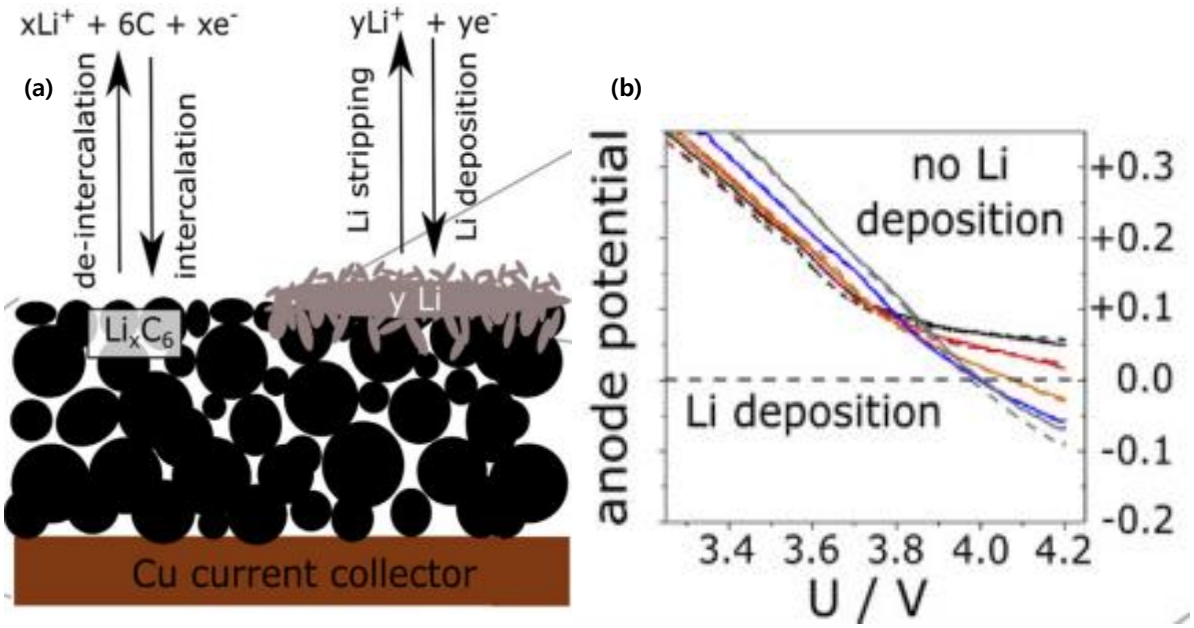

Figure 3. Scheme of Li deposition (a) on the microscopic level and (b) macroscopic level

The anode potential is one of the obvious signals to decide whether anode lithium plating occurs. Anode lithium plating occurs when the anode potential falls below 0 V (v Li+/Li)[3] as figure 3(b) showed macroscopic level.

Figure 3(a) showed Li deposition mechanism in the microscopic level. Li deposition occurs as an inter-parallel reaction. Charging process can lead to intercalation(quantity : x) and further Li deposition(quantity: y). Discharging process also can lead to de-intercalation and stripping of the deposited Li. At the microscopic level, there are two ways showing negative kinetics resulting Li deposition. One is when Li ions are moved between the anode openings which is associated with porosity and tortuosity. The other is when electrons are transferred from particles of the active material to the current collector.

This associates with not only the transfer of Li ions in the openings of the anode, [4,5] but also the transfer of electrons from the active materials to the current collector.

Table 1. Methods which give hints on Li deposition [8]

Method/Principle	Limitation	scale
Low CE	High precision devices needed	Macroscopic, cell level
Analysis of capacity fade/ change of slope in Arrhenius plot	Massive Li deposition	Macroscopic, cell level
Capacity recovery	Only if Li deposition partly reversible	Macroscopic, cell level
Voltage plateau during discharge	Low T area of Li deposition must be large enough	Macroscopic, cell level
Voltage curve shape during rest after charging	Low T area of Li deposition must be large enough	Macroscopic, cell level
Dilation, measurement of cell thickness	Limited to pouch cells, low T, superposition with gassing possible, massive Li deposition	Macroscopic, cell level
Early exothermic reaction in ARC tests	Massive Li deposition	Macroscopic, cell level
Fire during reaction with H2O	Reactivity of Li depends on its microscopic morphology and passivation	Macroscopic, electrode level
Melting point of Li, DSC	Melting point might be influenced by alloying	Macroscopic, electrode level
Dendritic structure	Microscopic morphology of Li depends on pressure in cell	Microscopic, electrode level
Neutron diffraction, LiC6 and Li C12 intensities	In direct evidence	Macroscopic, cell level
Li-NMR	Direct evidence	Microscopic, electrode level
GDOES	Semi-quantitative evidence	Macroscopic, electrode level
XPS	Direct evidence, limited to surface particles	Microscopic, electrode level

Several hints for Li deposition are listed in the table 1 above. Table 1 showed various method ranging from Arrhenius plot to XPS investigating various scale from cell level to electrode level. Among many hints of Li deposition, the first one of them, Coulombic efficiency, was noted. The increased aging rate is mirrored in the Coulombic efficiency. (CE), which means the proportion between charge capacity and discharge capacity. If the capacity is more charged than discharged, the difference of charging value affects the reaction separately not the process of Li intercalation and de-intercalation [6,7]. Some cases of side effects are growth of SEI layer or the response between electrolytes and electrodes. Also, decreased electrical interaction of the active material or increased resistance leads to film establishments. Film establishments and pore congestion can furthermore contribute to capacity loss. Dahn's group

developed high precision coulometry.

Graphite remains still promising anode material due to low cost compare to showing high capacity and suitable voltage profile complex compare to others. However, Li plating on the graphite appears during rapid charging.

The requirements for improving Li ion battery issues currently are longer lifetime, rapid charging, stable charging for low temperature. Also, the safety performance accompanied.

1.2.2 Sand's time

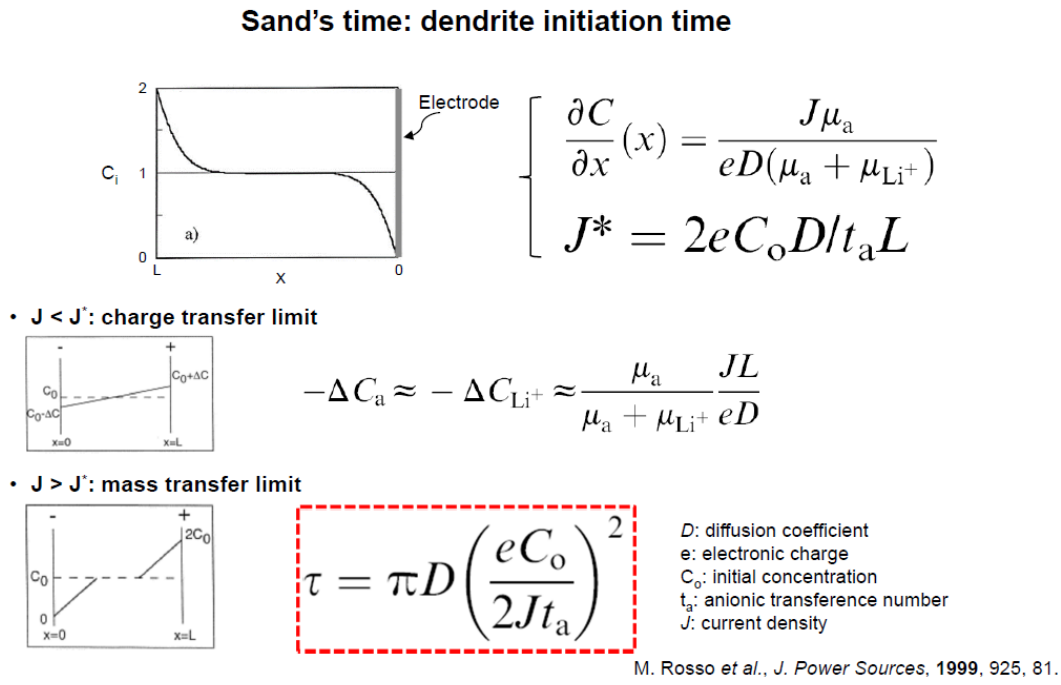

Figure 4. Sand's time which means initiation time of dendrite [10]

As a broadly known diffusion template, the relationship between the sand's time and the transfer characteristics of lithium ions and the transfer characteristics of electrons is as follows.

τ is the time when Li dendrites start to grow.

The SEI layer affect the mobility of Li ions to play a title role in the Sand's time. Also, the movement of electrons involve the effective current density, which affects the sand's time. When the mobility of Li ion gets bigger and effective current density (J) gets smaller and smaller, sand time (τ) get bigger. It

means that the cell has a long lifetime [9]. Thus, Sand's template can relate properties layer ranging from SEI layer to electrode.

Subsequently, people have effort to decrease the local current density when the large bulk current flows into the Li deposition sites which guarantee the fast charging rate of cells [9]

1.2.3 Control the current density

$$\tau = \pi D \left(\frac{eC_o}{2Ji_a} \right)^2$$

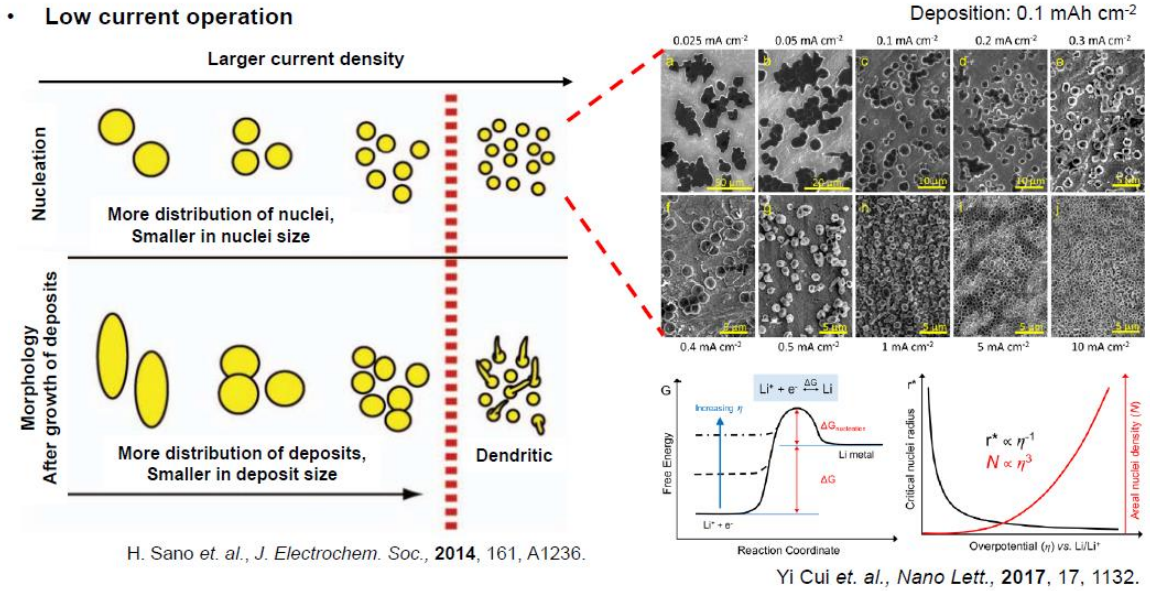

Figure 5. Schematic of the effect of current density on the distribution of Li nuclei and Lithium nuclei deposited at different current densities[11,14]

Figure 5 illustrates that current density controls the distribution of the lithium nuclei and decides the morphology of the lithium deposits. Especially, fast charging whose current density is high made Sand's time become shorter. It made Li nuclei frequently scattered and Li dendrite structure. When the larger current flows, the current density gets higher. As a result of higher current density, the nuclei are further scattered, and the size of the nuclei is reduced, and form of nuclei change into dendritic structure. When the smaller current flow, the current density gets smaller. As a result of smaller current density, the nuclei are grown and deposited semi-spherically and the deposition turns into condition of charge-transfer controlled. [11] In order to delay the dendrite initiation time, the region for control the charge-

transfer controlled needed. When a much huge current flow, the deposition turns into condition of diffusion controlled. Also, the rate of diffusion of lithium ions is much slower than the Li-ion reduction, which make the potential extremely negative numbers and lithium deposition come to be central reaction. [12,13] For suppressing Li dendrite formation, the appropriate value of current density should be in the model of charge transfer controlled growth.

The nucleation of Li metal on Cu and the dependence of lithium nuclei range, form, and areal current density can be cooperate with current rate. According to Yi cui s group, the Li cores range is disproportionate to the overpotential and the number density of nuclei is proportionate to the cubic power of overpotential.[14]

1.3 Research about fast charging

When charging the battery excessing 2C rates, various electrochemical phenomena will result constrained accessibility of the active material, increased inclination towards Li plating, and extreme heat generation.

Considering the demands developed at the battery level in relation to high-speed charging, each lithium-ion battery requires optimized research. The important direction is to improve the transfer characteristics of the electrolyte, reduce the diffusion distance through electrode structure design, reduce the tendency of Li plating through detailed charging methods, integrate functional detection within the battery, develop an advanced temperature control system, and evenly extract heat from the battery.

The behavior of cells and packs undergoing rapid charging depends on various factors. As shown in Figure 6, it scales from the atomic level to the system level.[15]

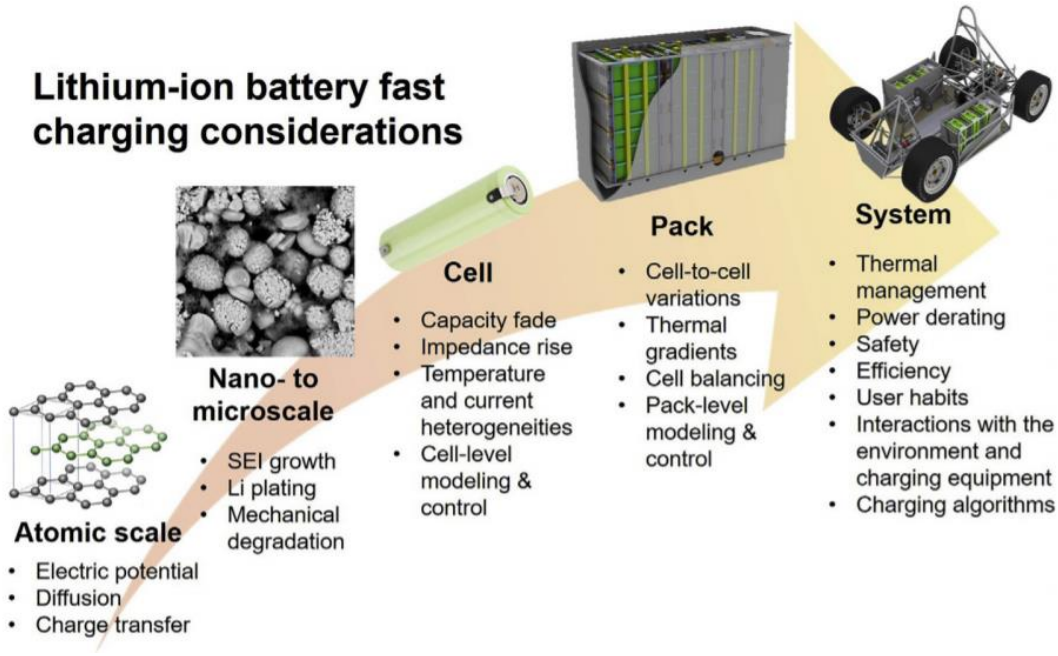

Figure 6. Crucial factors concerning Li ion battery rapid charging at different scales

Rapid charging capability has become crucial points besieged by battery and electric vehicle industries. However, rapid charging has been shown to speed up aging of cells, causing mutually the capacity fading and worsen power capability. Low temperatures issues, which is spotlighted in many crucial EV fairs deteriorate even further because of the sluggish diffusion of Li ions between the electrodes and the electrolyte and the slow-moving reaction of intercalation

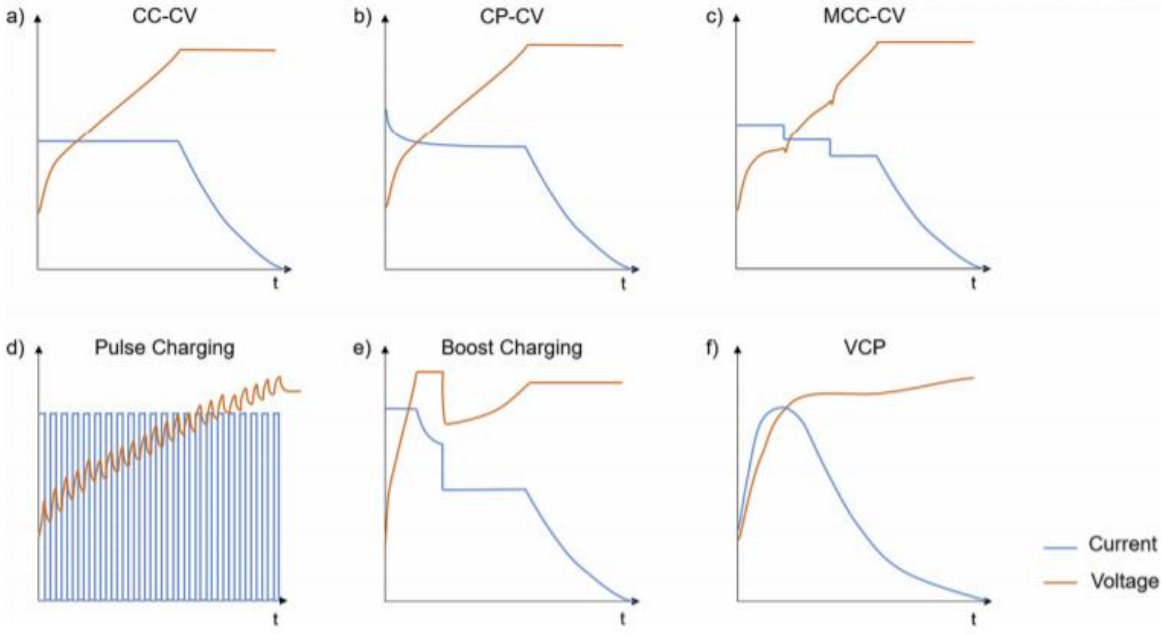

Figure 7. Depiction of ordinary types of charging protocols proposed for fast charging. a) Constant Current - Constant Voltage (CC-CV), b) Constant Power – Constant Voltage (CP-CV), c) Multistage Constant Current - Constant Voltage (MCC-CV), d) Pulse charging, e) Boost charging with a CC-CV-CC-CV scheme, f) Variable Current Profile (VCP,)

Figure 7 showed various charging protocol for suppressing side reaction of fast charging. Among various charging protocol, multi-stage constant current (MCC) protocol and boost charging protocol were selected. The process of modifying the current during charging can regulate cell degradation while lowering charging rate. This protocol is often decided by avoiding the mechanical stress surroundings when Li plating occurs by dropping heat generation.[16]. The MCC protocol is one of the initial sorts specially devised for rapid charging. These procedures have two or more constant current steps, afterward a CV steps follow. Higher current levels are generally selected for the preliminary CC step as the anode potential less grow to be negative when charging occur.

Boost charging features a CC-CV part with a higher average current at the start of charging and then a more moderate current. The first boost charging step is simply a CC profile, a CV profile where the cell immediately reaches its set maximum voltage via a high initial current (CV-CC-CV), or a full CC-CV profile (CC-CV-CC-CV). In any case, boost charging stage should allow for a higher current or higher maximum voltage compared to the next CC-CV section to reduce the total charging time[16].

II. Experimental Method

2.1. Electrode and cell fabrication

The active material of negative electrode and positive electrode separately were S360 graphite and NCM811(Slab Co., Ltd.). The anode material with the total ratio of 2.6% binders were mixed. Binders were 1.2% CMC (MAC350H, ZEON) with 1.4% SBR (BM-451B, ZEON). The active material and binder were mixed in homogenizer (NISSEI) with 12000rpm for 1 hour. The Slurry of mixed anode complex was covered with loading on the Cu substrate whose thickness is 18um and coating has a loading level of 10.0mg/cm^2. Dry process was done in the 80ºC oven for 1 hour. Pressing process was done with dried anodes ranging from 1.5g/cc to 1.7g/cc. Vacuum- dried in the 110ºC oven for 10 hours.

NCM811 single crystal with PvdF(KF9300, Kureha) binder and two different conducting agents were mixed. One is consisted of 3 wt% carbon black (VGCF, TIMCAL) and the other is 1.5 wt% SFG6 (TIMCAL). Also, PvdF is 2 wt% of a polyvinylidene fluoride (KF9300, Kureha) binder. The active material ratio was fixed as 94%. The cathode slurries were mixed using homogenizer (NISSEI) with 10000rpm for 1-hour 30minute. The Slurry of mixed cathode complex was covered with 15.2mg/cm^2 loading level on the 15um Al substrate. Dry process done in the 110ºC oven for 1 hour. Pressing process was done with dried electrodes with 3.4g/cc. Vacuum- dried process was done in the 110ºC oven for 10 hours.

The cathode electrode and anode electrode were fabricated in the form of 2032 coin half-cell and in the form of pouch full-cell. Coin cell were constructed in the glove box and pouch cell in the dry room. Electrode were pierced for all same size in 14pi-size for testing coin half-cell. For pouch full-cell, cathode was pierced in the size of 20mm*25mm and anode was pierced in the size of 22mm*27mm. The electrolyte applied for coin half-cell and pouch full-cell is 1.15M $LiPF_6$ dissolved in mixed organic solvents, comprising ethylene carbonate (EC), Dimethyl carbonate (DMC), in the volume ratio of (EC:DMC) 5:95 with additives of 10% fluoroethylene carbonate (FEC, Enchem) and 1% Tris(trimethylsilyl) phosphite (TMSP, Sigma Aldrich) from Professor Choi's group. Separator was PP/PE/PP whose thickness was 20um (Celgard)

The pouch cells 48mm length x width and the composition of the pouch cell was as follow. Cathode:20mm*25mm , Anode:22mm*27mm ,Separator:26mm*30mm.

Cell balancing: 1.10

2.2. Physical characterization

With Scanning Electron Microscope (SEM,Nova NanoSEM,FEI) the anode and cathode before the cycle and the anode and cathode after the cycle were observed. Before sampling in the SEM holder, the pouch full cell was disassembled in the dry room, and the anode and cathode were washed with DMC solution to remove remaining salt.

Using Ion milling (IM400, HITACHI), cross-section of cathode and anode are gained. Ion milling were done for 1.5 hour. The current of Ion beam is 110uA and gas flow is 0.15cm^3/min.

2.3. Chemical characterization

X-ray photoelectron spectroscopy (XPS,K-alpha, ThermoFisher) analysis was requested to analyze the surface of the layer laminated on the graphite. XPS analysis is performed in ultra vacuum (<1.3 x 10-8 Pa) state and depth profiling by 500V Ar ion sputtering. Like SEM analysis, the cell was disassembled and then returned to the XPS room.

The cathode was subjected to X-ray diffraction (XRD, HRPXRD, RIGAKU) to examine phase clarity and decide crystal building. XRD test done under Cu Kα radiation (λ = 1.54056 Å) at 40 kV and 30 mA. For the phase identification, the scanning 2θ scope was established from 10° to 70°, with a scanning rate of 0.04° s^{-1}.

2.4. Electrochemical test

The charging and discharging of the rechargeable battery were conducted with cycler (PESC 05-0.1, PNE SOLUTION). The voltage range is between 2.8V and 4.2V, and formation process was conducted at 0.1C charge and 0.1C discharge at 25 degrees. Standard processes were conducted at 0.2C charge and 0.2C discharge at 25 ℃

High-rate charging were done by dividing single stage Charging and double stage charging ranging from 3C charging to 5C charging. In the single stage charging method, after 10 minutes of rest in a cell discharged to 2.8V, charging with CC mode occurred up to 4.20V at 3C or 5C, and then proceeded CV mode so that the cut-off current drops to 1/20C. In the double stage charging method, after 10 minutes of rest in the cell discharged to 2.8V, charging CC mode up to 4.19V with 3C or 5C, and then proceed CV mode so that cut off current dropped to 1/30C in and then re charging CC mode up with 1/30 C to 4.20V as shown in figure 8. Cut off current in CV mode was 1/20 C. The current density is 2.72 mA/cm2 at discharge, 8.16 mA/cm2 at 3C charging and 13.6mA/cm2 at 5C charging.

Single stage charging

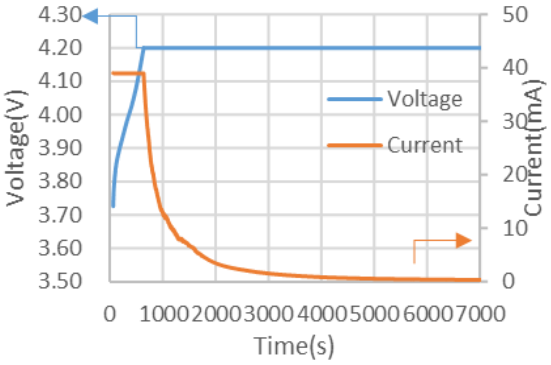

Double stage charging

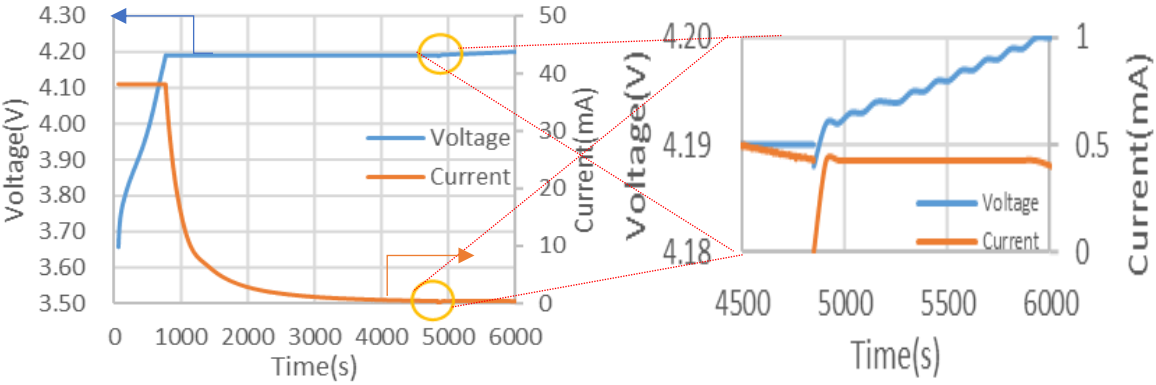

Figure 8. 2 type of charging protocol of rapid charging

III. Result and discussion

3.1 Electrochemical tests

3.1.1 Formation and standard process

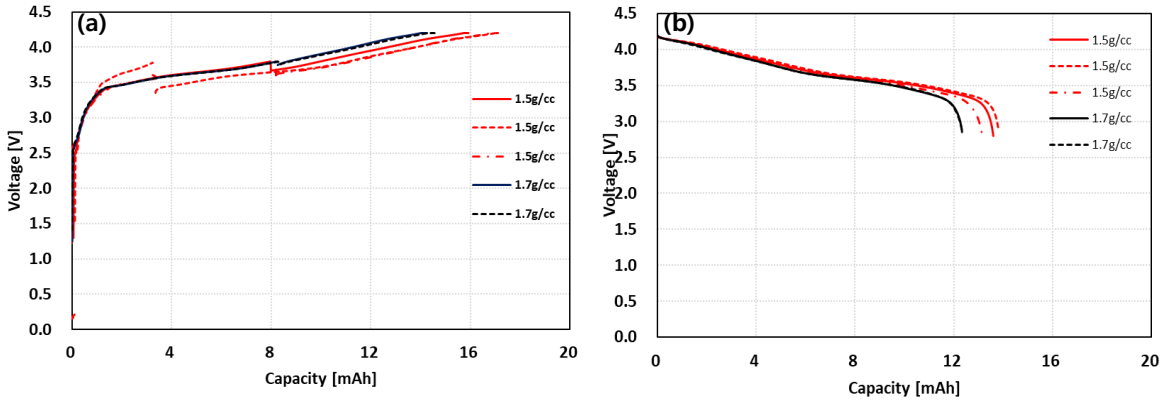

Figure 9. Formation (a) Charging data of Full cell 1.5g/cc and 1.7g/cc (b) Discharging data of Full cell 1.5g/cc and 1.7g/cc

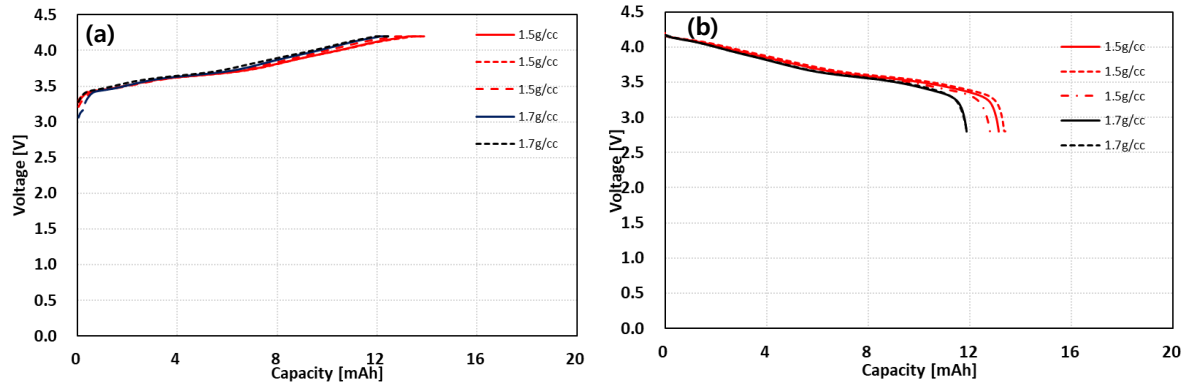

Figure 10. Standard (a) Charging data of Full cell 1.5g/cc and 1.7g/cc (b) Discharging data of Full cell 1.5g/cc and 1.7g/cc

Figure 9 showed the graph of formation with pouch full cell. In formation process, the average charging capacity and discharging capacity of anode samples whose electrode density is 1.5g/cc was separately 16.63mAh and 13.59mAh while average charging capacity and discharging capacity of anode sample whose electrode density is 1.7g/cc was 14.56mAh and 12.35mAh. The average ICE of anode samples whose electrode density is 1.5g/cc was 81% while that of anode sample whose electrode density is 1.7g/cc was 85%. Discharging capacity of anode sample whose electrode density is 1.5g/cc show on average as high as 1.16mAh than that of 1.7g/cc. Figure 10 showed the graph of standard with pouch full cell. In the standard process, The average charging capacity and discharging capacity of anode samples whose electrode density is 1.5g/cc was separately 13.75mAh and 13.08mAh while average charging capacity and discharging capacity of anode sample whose electrode density is 1.7g/cc was 12.38mAh and 11.87mAh. CE of cell with an anode of 1.5g/cc showed an average 96% and cells with an anode of 1.7g/cc had an average of 95%. Discharging capacity of anode sample whose electrode density is 1.5g/cc show on average as high as 1.46mAh than that of 1.7g/cc

3.1.2 Cycle life test on high rate charging

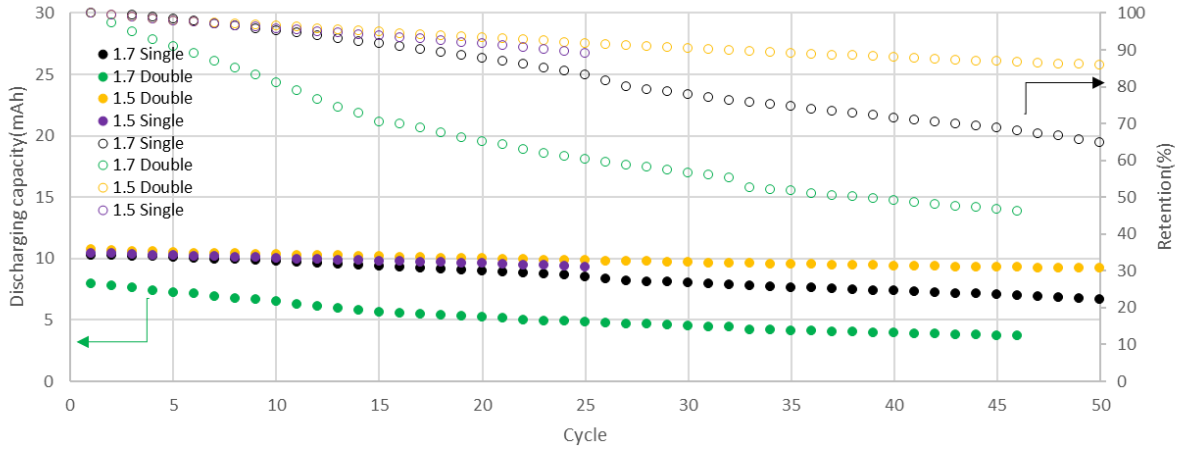

Figure 11. Discharging capacity and retention of 3C charging 1C discharging Cycle life test

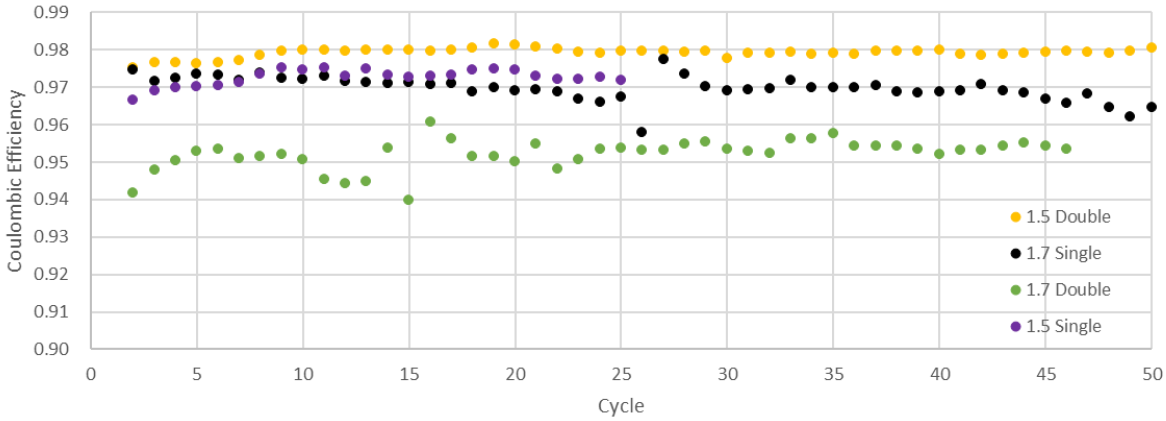

Figure 12. Coulombic Efficiency graph when 3C Charging 1C Discharging

Figure 11 showed discharging capacity and retention when 3C charging and 1C discharging cycle life test done. Figure 12 showed the coulombic efficiency when 3C charging and 1C discharging cycle life test done. In the case of a cell with 1.5g/cc anode, the cell discharged at 1C and charged at 3C in a double stage. Discharging retention was more than 80.0% in the 50th cycle, and coulombic efficiency was also higher than other cells. After the 5th cycle, the coulombic efficiency showed steadily 97.6%. In the case of a cell with a 1.7g/cc anode, the cell discharged at 1C and charging at 3C in a double stage. The discharging retention was 49.1% at the 40th cycle, and the value of coulombic efficiency was between 95.0% and 96.0% after the 20th cycle. In the case of a cell with 1.5g/cc anode and discharged at 1C charged 3C in a single stage, discharging retention was more than 89.2% in the 25th cycle and value of coulombic efficiency was between 97.0% and 98.2% after 5 cycles

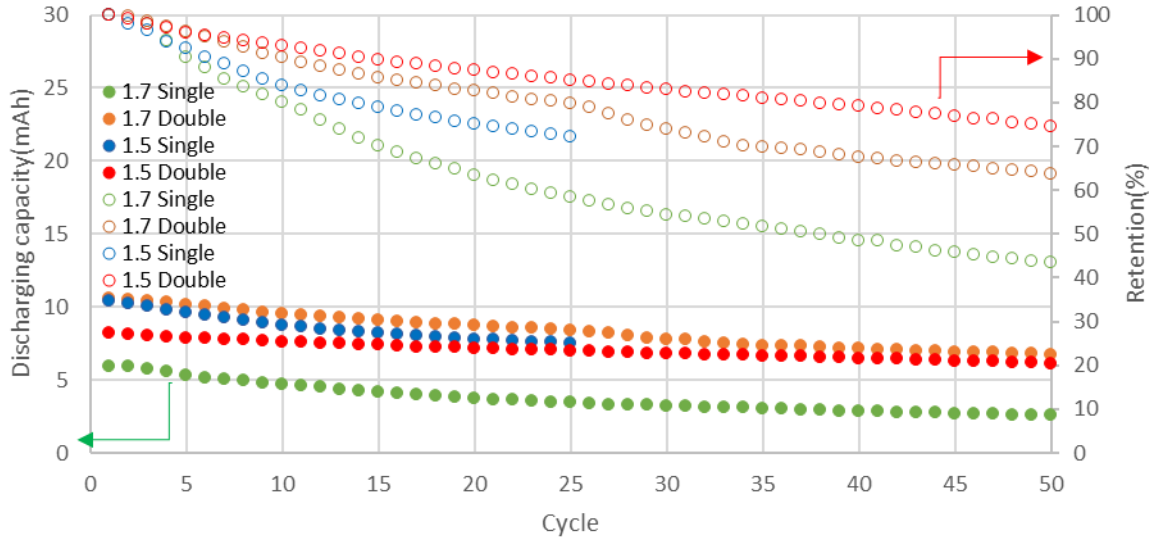

Figure 13. Discharging capacity and retention of 5C charging 1C discharging cycle life test

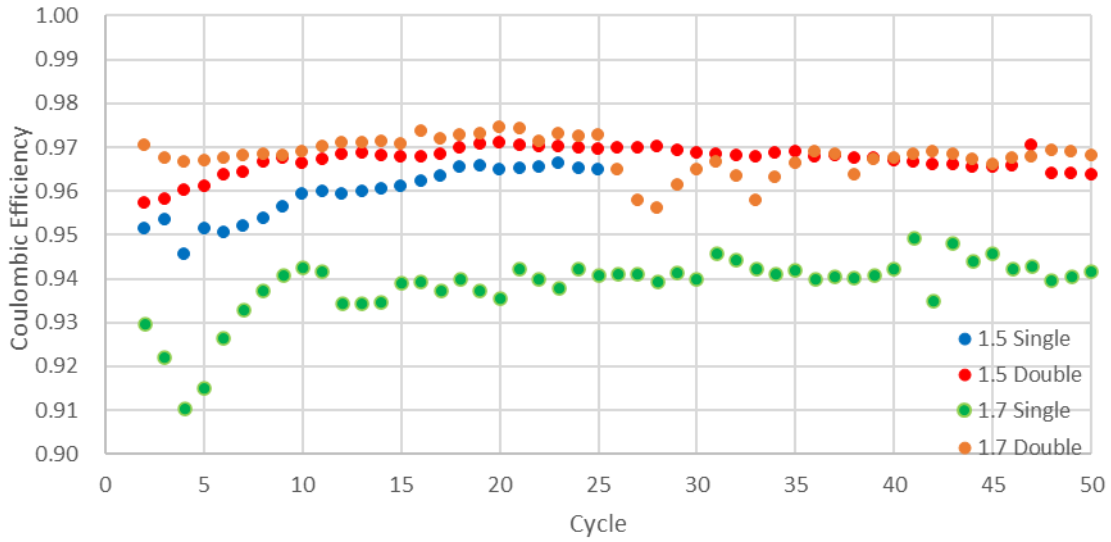

Figure 14. Coulombic Efficiency graph when 5C Charging 1C Discharging

Figure 13 showed discharging capacity and retention when 5C charging and 1C discharging cycle life test done. Figure 14 showed the coulombic efficiency when 5C charging and 1C discharging cycle life test done. In the case of a cell with 1.5g/cc anode, the cell discharged at 1C and charged 5C in a double stage. The discharging retention is 74.5% at 50th cycle. After the 5 cycle, the coulombic efficiency showed steadily 97.0%. In the case of a cell with 1.7g/cc anode and discharged at 1C and charged 5C in double stage. The discharging retention was 63.7% at the 50th cycle and value of coulombic efficiency was 97.2% from the 10th cycle and 25th cycle.

In the case of a cell with 1.5g/cc anode, the cell discharged at 1C and charged 5C in a single stage. The discharging retention was more than 72.1% in the 25th cycle and value of coulombic efficiency was between 96.0% and 97.0% after 10 cycles

3.1.3 Compare charging time between single stage and double stage charging

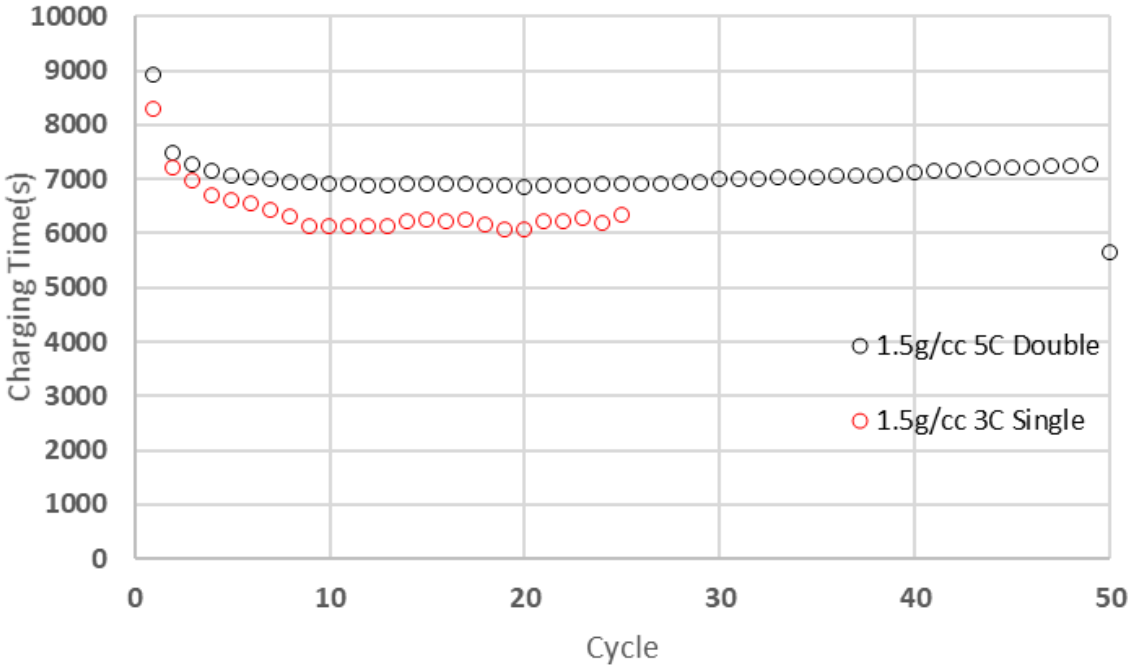

Figure 15. Charging time vs Cycle graph on high rate charging of 1.5g/cc anode

Figure 15 shows the 5C double stage charging time and the 3C single stage charging time for each cycle in a full cell with the same anode of 1.5g/cc. Looking at the chart from 10 cycles to 25 cycles, 5C double stage charging takes about 1000 seconds per cycle than 3C single stage charging.

Figure 16 shows the 5C double stage charging time and the 3C single stage charging time for each cycle in a full cell with the same cathode of 1.7g/cc. The charging time of 3C is constant per cycle, but the charging time increased by as much as 2000 seconds from 25 cycles in the 5C double stage charging method. From the 25th cycle, the deterioration rate increased and the charging time increased due to Li deposition and Li striping.

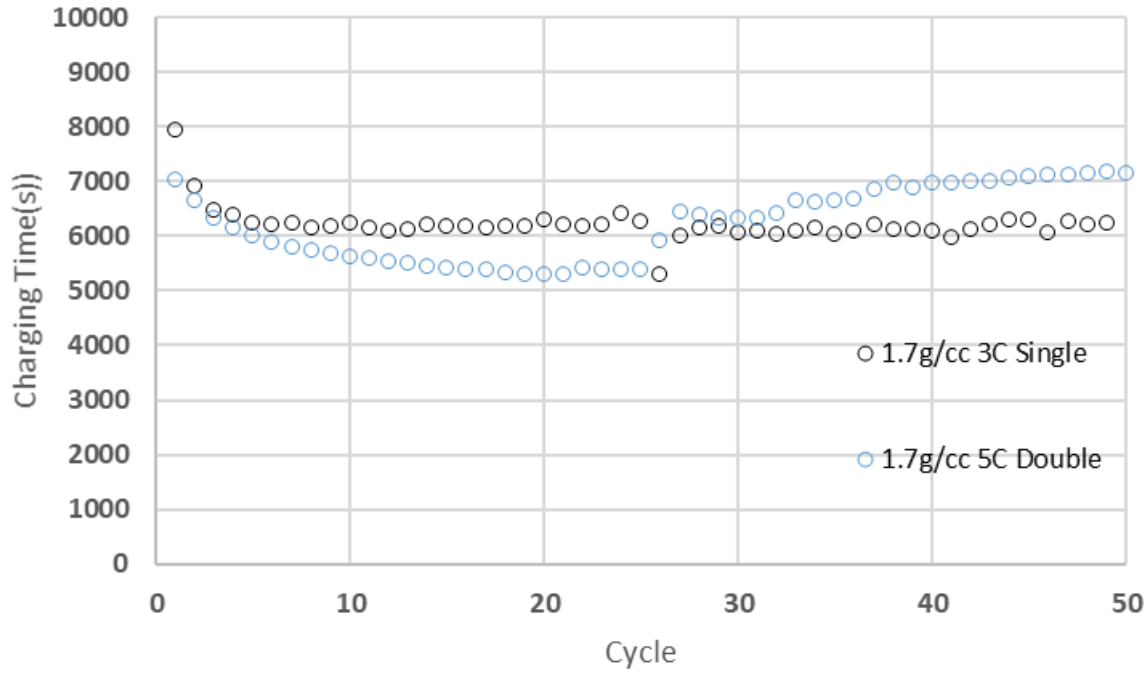

Figure 16. Charging time vs Cycle graph on high rate charging of 1.7g/cc anode

3.2 SEM/EDX/XRD/XPS analysis and wettability test

3.2.1 SEM and EDX analysis

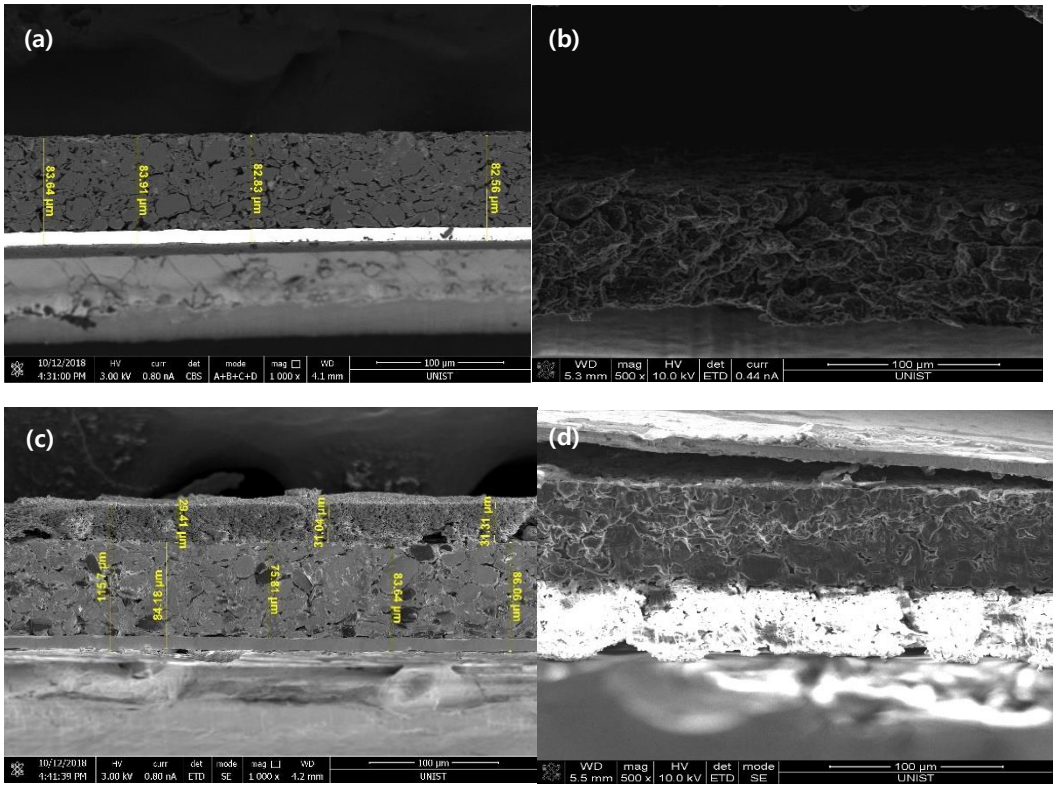

Figure 17. Cross section image of (a) Pristine graphite, (b) graphite showing good retention(3C), (c) graphite showing Bad retention(3C) and (d) graphite of 5C charging

The graphite sample was disassembled in the dry room and observed with SEM. Figure 17(a) is a pristine graphite, and figure 17 (b) is a 1.5g/cc graphite, taken in a charged state after 50 cycles of 3C double stage charging and 1C discharging. Unlike other anodes with Li deposition, there is no lamination structure. On the other hand, figure 17 (c) and figure 17 (d) are respectively 1.7g/cc graphite sample. (c) taken in a charged state after 50cycle, 3C single stage charging and 1C discharge. (d) showed the sample which undergo 50 cycles 5C single stage charging and 1C discharge. After 50 cycles of 5C single stage charging and 1C discharging, a new stacked structure was created. This can be a Li dendrite layer. In Figure 18(a), the layered structure was confirmed by mapping through EDX in the form of Oxide. On the other hand, in figure 18(b), the thickness of the layered structure is relatively thin, and there is no oxide form, and it is a thin compound with F.

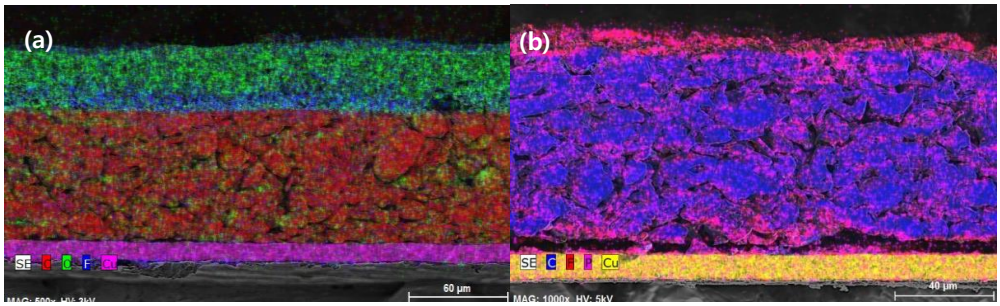

Figure 18. EDX mapping image of graphite showing (a)Bad retention(3C) and (b)good retention(3C)

Table 2. EDX mapping color of element

	O	F	C	Cu
(a)				
	P	F	C	Cu
(b)				

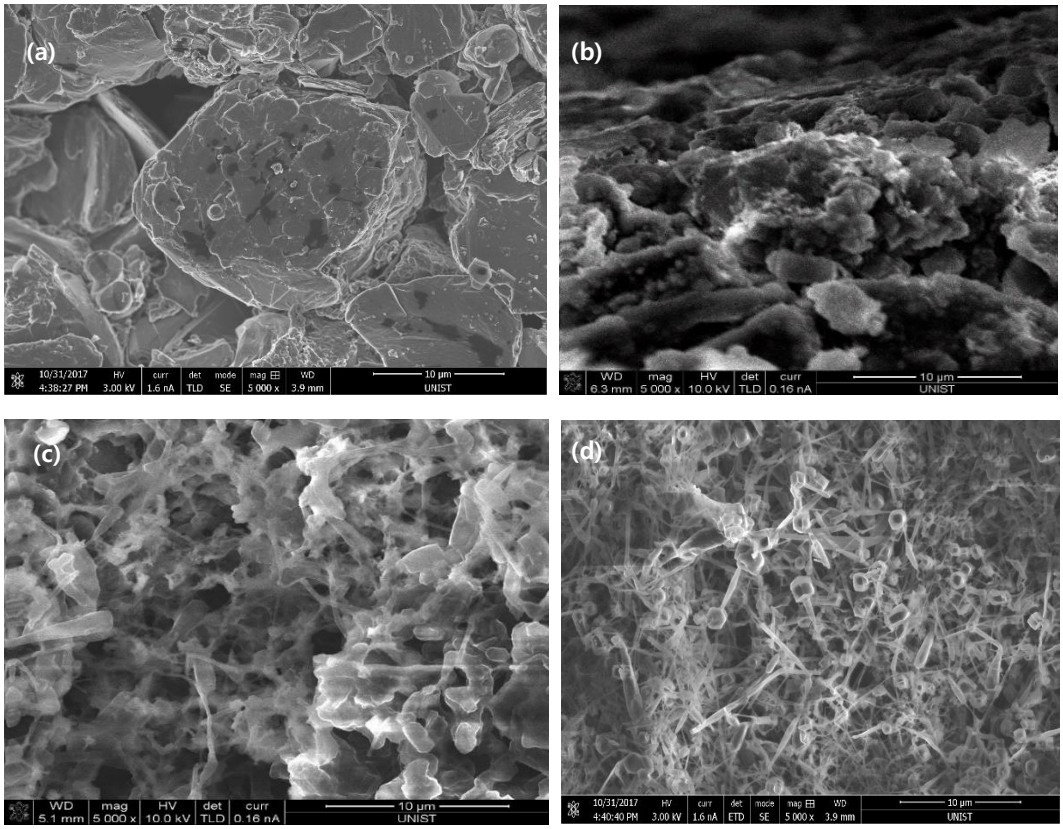

Figure 19. Surface image of Pristine graphite ,graphite showing good retention(3C), graphite showing Bad retention(3C) and graphite of 5C charging

Figure 19(a) is a surface image of pristine graphite, and figure 19(b) is image of a 1.5g/cc graphite, taken in a charged state after 50 cycles of 3C double stage charging and 1C discharging. Unlike other anodes with Li deposition, there is no lamination structure. On the other hand, figure 19 (c) and figure 19 (d) are respectively 1.7g/cc graphite sample. Figure 19 (c) and figure 19 (d) showed Li dendrite form taken in a charged state after 50cycle

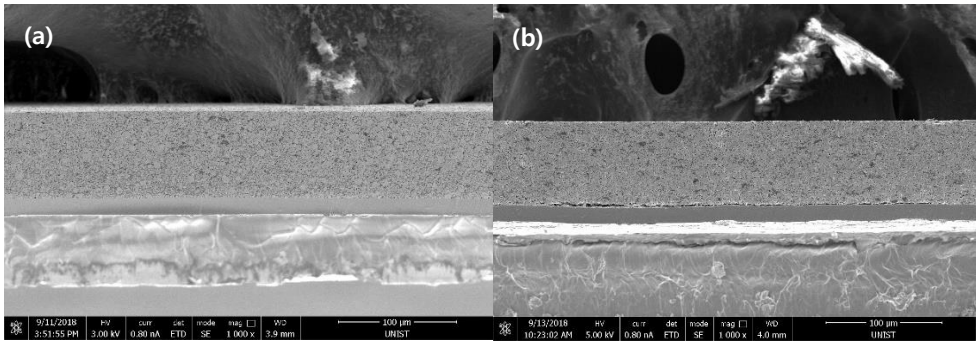

Figure 20. NCM811 cross-section image(a) pristine (b) after 5C 50cycle

On the other hand, from Figure 20, the cross section of NCM811 does not show much difference before and after the cycle without any reactants. In Figure 21, there were also several photographs of the NCM811 surface. There was no substantial change between pristine image and image of rapid charging other than the binder agglomeration phenomenon.

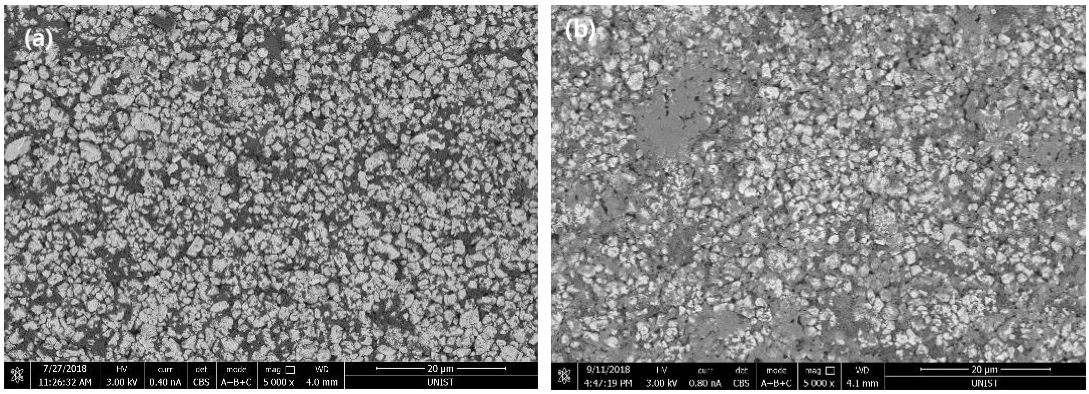

Figure 21. NCM811 Surface image (a) pristine (b) after 5C 50 cycle

3.1.2 Wettability test

The contact angle was measured by dropping 2ul of electrolytes on a graphite electrode plate of 3.4 g/cc anode NCM 811 and anode densities of 1.5 g/cc and 1.7 g/cc, respectively, at room temperature. Since the wettability of the electrolyte solution is high, the contact angle of the image taken that moment of dropping was measured. Figure 22 showed that on average the cathode had a contact angle of 17.93°, the average of 1.5g/cc graphite was 17.8°, and the 1.7g/cc graphite was 16.1 °. The lower the contact angle, the better the impregnation, and it was found that impregnation was slightly different depending on the density of the anode.

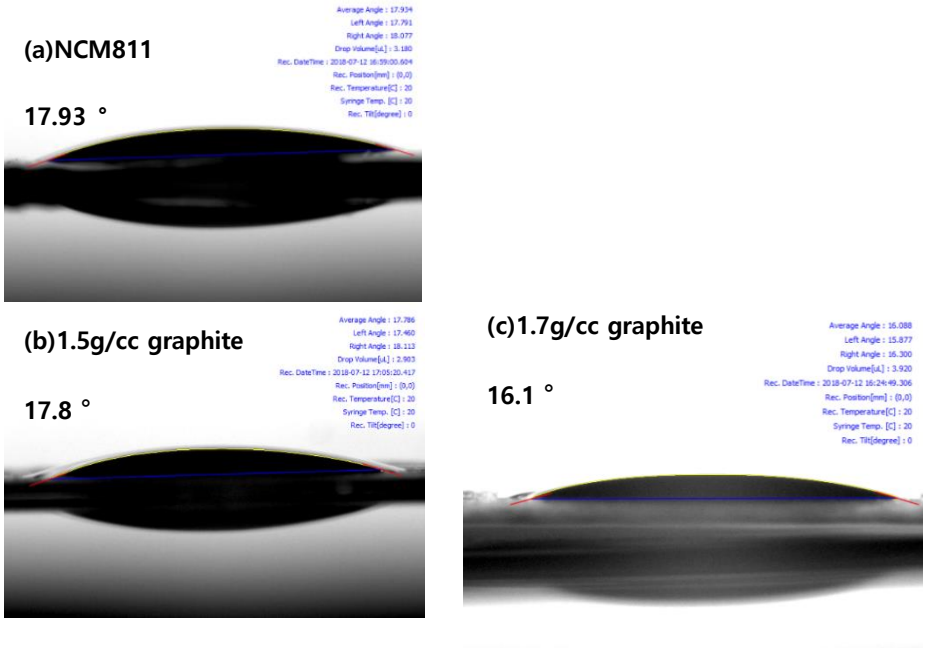

Figure 22. Contact angle measurement of cathode material and anode material

3.1.3 XRD analysis

For ex-situ XRD measurements, the cycled electrodes disassembled and washed with DMC solvent for numerous moments and dried in a dry room. The dried electrodes were transformed with a thin PE film to make an ex-situ XRD cell.

Figure 22 showed the XRD pattern. Figure 22(a) showed the pattern of cell after 3c 10cycle and figure 22(b) showed the pattern of cell after 3c 30cycle and figure 22(c) showed the pattern of cell after 0.1c after 1cycle. X-ray diffraction (XRD) pattern was done to examine the structural changes of the cathode before cycling and after cycling. The (003) diffraction peak for the cathode after two fast charging cycles shifts at a lower angle compared to the cathode before fast charging. The distance between the layers of the cathode increases significantly after cycling. The I(003) /I(104) Intensity ratio is over 1.2, which indicates that the cation mixing between Li^{+} and Ni^{2+} is low (respectively 1.4347, 1.4831 ,1.1210).[17,20]

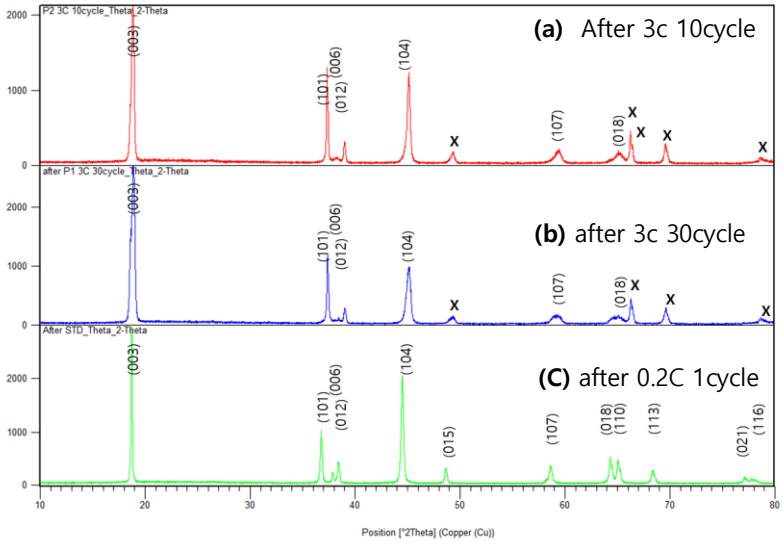

Figure 23. XRD pattern for NCM 811 electrode after cycle

3.1.4 XPS analysis

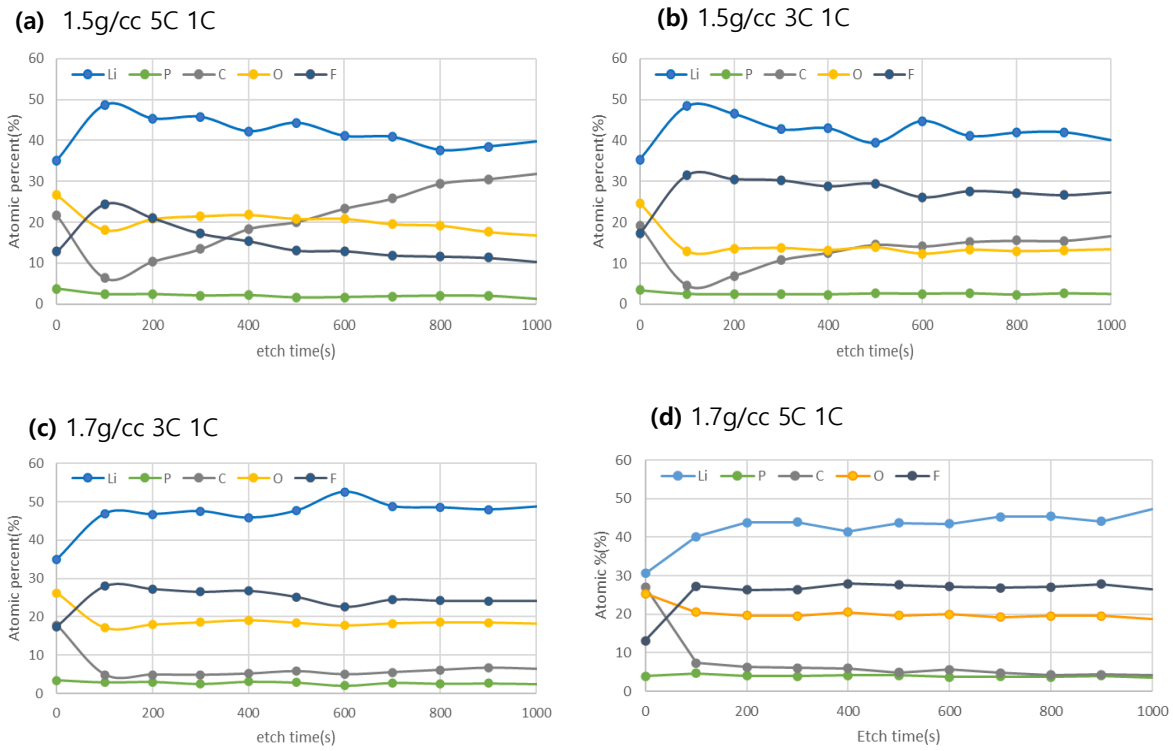

Figure 24. Atomic percent of each element of Li, P, C, O, F by depth profiling (a) 1.5g/cc 3C charging 1C discharging (b) 1.5g/cc 5C charging 1C discharging (c) 1.7g/cc 3C charging 1C discharging (d) 1.7g/cc 5C charging 1C discharging

As a result of quantitative analysis of this sample subjected to depth profiling, the atomic percent can be confirmed in the following Figure 24. Overall, the Li ratio is 40-50% after high-speed charging.

Speaking of depth profile information, eliminating substance from the surface using Ar^+ ion sputtering is very abusive and can lead to toughness due to sputtering, favored elimination of some elements and break down of compositions. Therefore, the several effects of sputtering on the compounds related in anode measurements were analyzed individually. One essential result is the creation of Li_2O because of Li_2CO_3 decomposition. $LiPF_4$ decomposed to form a small amount of LiF. The inserted LiC_6 electrode was not balanced during sputtering, so Li-OH was deposited on the surface.[18]

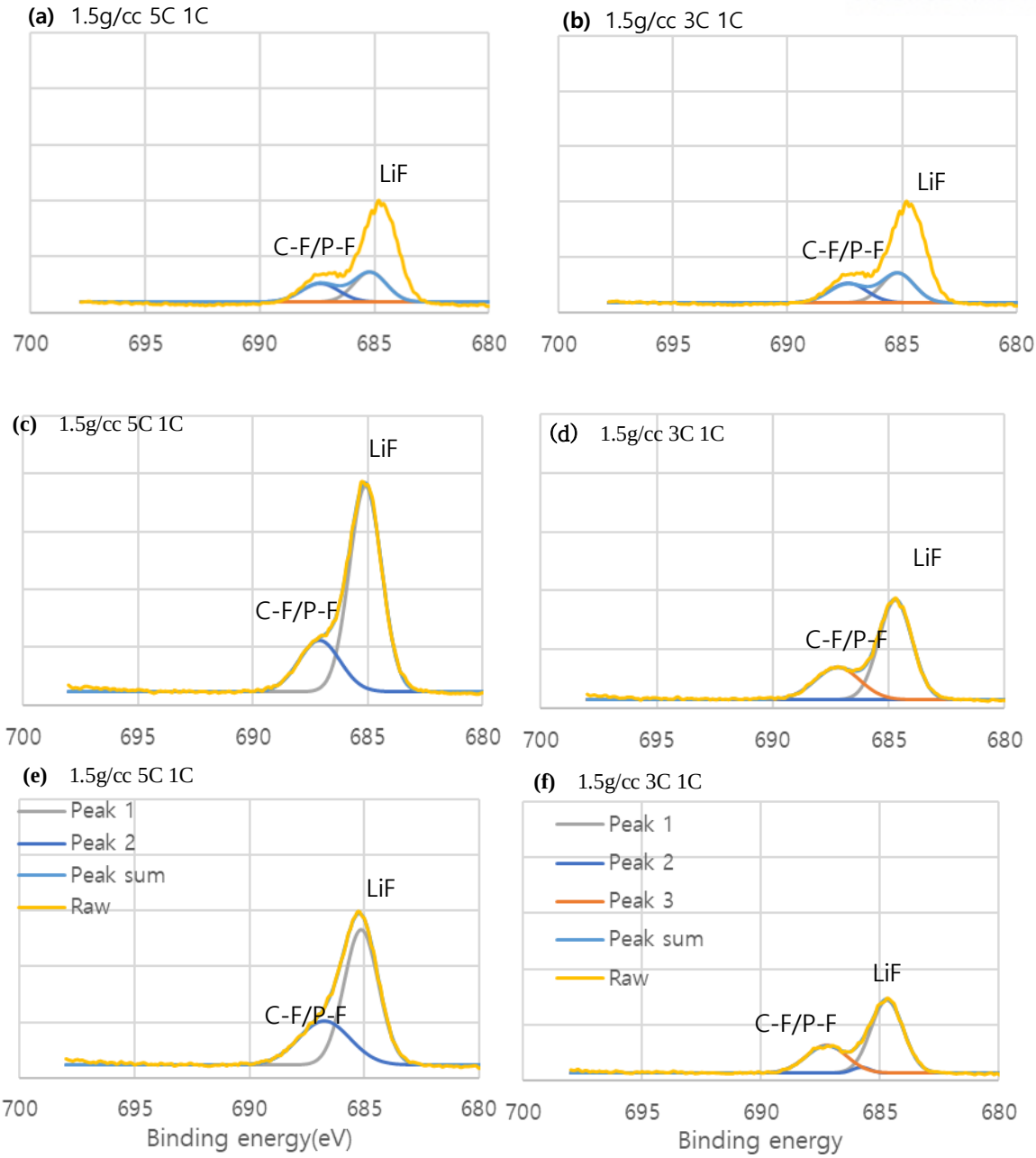

Figure 25. F 1s XPS spectra of anode (a) 1.5g/cc 5C charging 1C discharging depth profiling 0s (b) 1.5g/cc 3C charging 1C discharging (c) 1.5g/cc 5C charging 1C discharging depth profiling 200s (d) 1.5g/cc 3C charging 1C discharging depth profiling 200s (e) 1.5g/cc 5C charging 1C discharging depth profiling 1000s (f) 1.5g/cc 3C charging 1C discharging depth profiling 1000s

The figure 25 and 26 showed XPS spectra of F 1s. The first of 687.0 eV is due to the salt $LiPF_6$ and the second of 685.0 eV is assigned to Li-F. The overall amount of LiF increase as sputtering continue up to 1000s. During charging, an increase in the Li-F peak can be observed as the sample which were charged state were detected in the XPS room. The evolution of this spectrum is due to the deposition of a significant amount of LiF, which is a major component of the exterior part of the SEI layer. It can be inferred that the LiF layer, an important element of the SEI layer, is maintained through the tendency of the LiF amount to be found more during the depth profiling process.

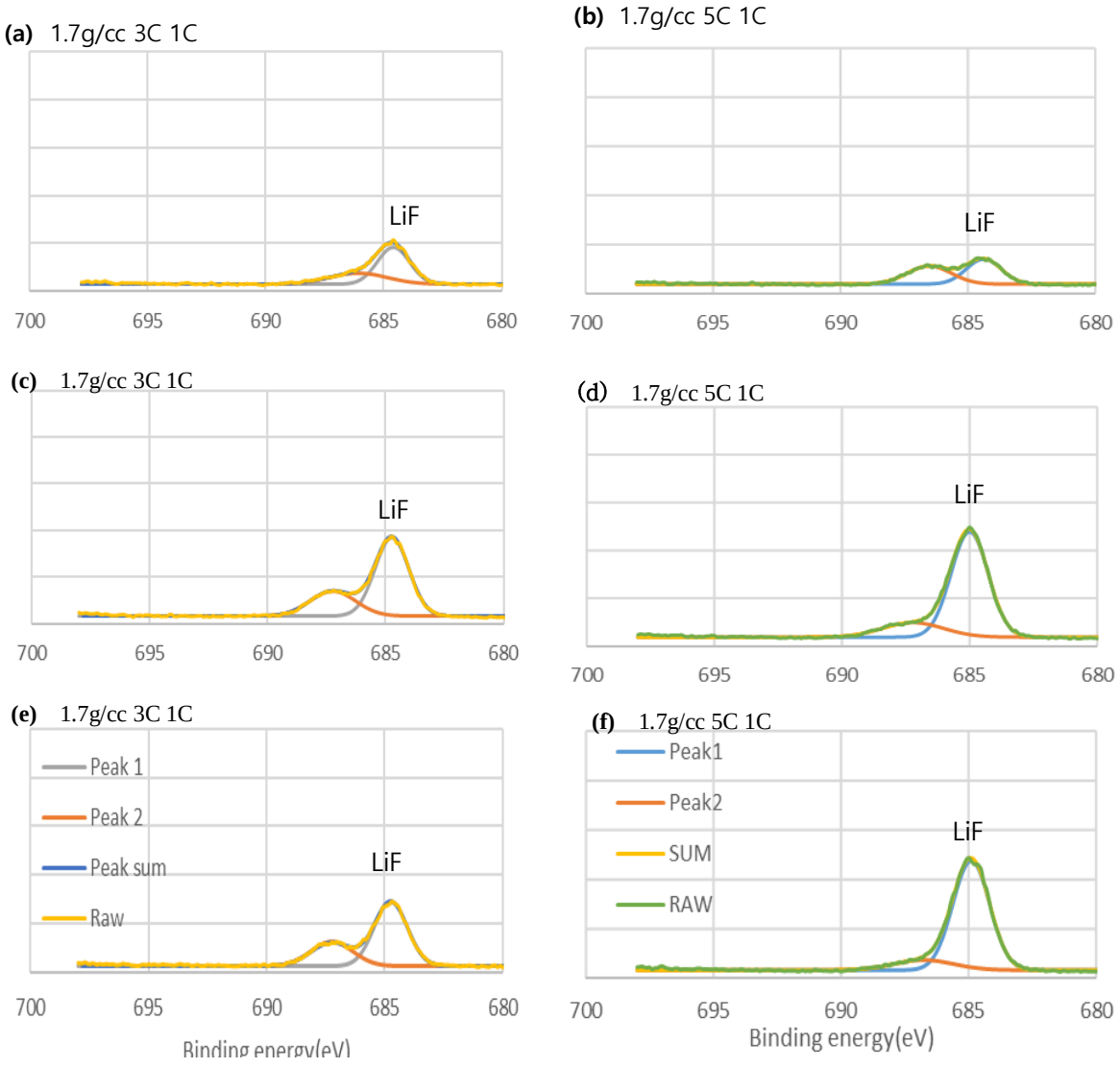

Figure 26. F 1s XPS spectra of anode (a) 1.7g/cc 3C charging 1C discharging depth profiling 0s (b) 1.7g/cc 5C charging 1C discharging (c) 1.7g/cc 3C charging 1C discharging depth profiling 200s (d) 1.7g/cc 5C charging 1C discharging depth profiling 200s (e) 1.7g/cc 3C charging 1C discharging depth profiling 1000s (f) 1.7g/cc 5C charging 1C discharging depth profiling 1000s

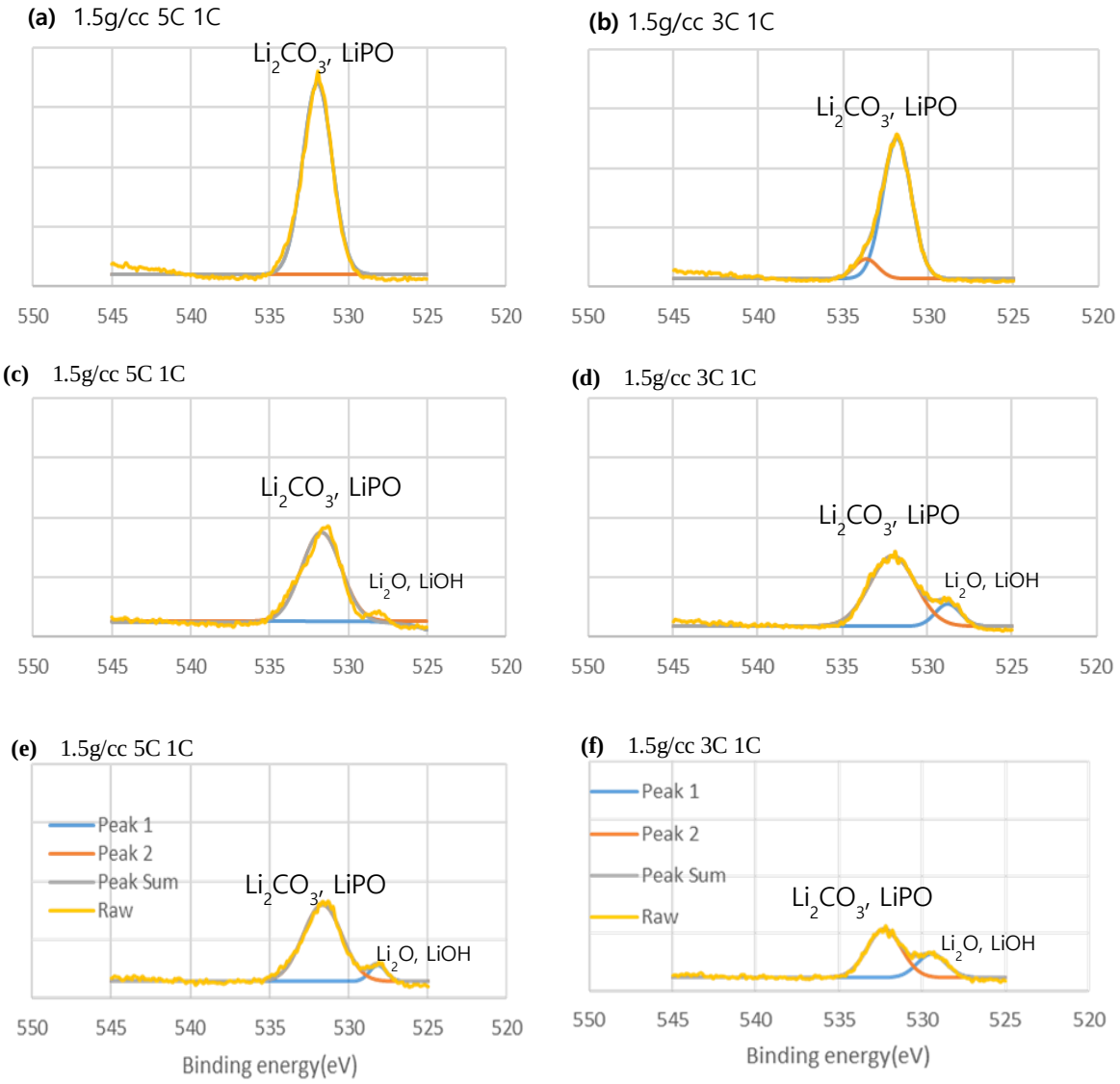

Figure 27. O 1s XPS spectra of anode (a) 1.5g/cc 5C charging 1C discharging depth profiling 0s (b) 1.5g/cc 3C charging 1C discharging (c) 1.5g/cc 5C charging 1C discharging depth profiling 200s (d) 1.5g/cc 3C charging 1C discharging depth profiling 200s (e) 1.5g/cc 5C charging 1C discharging depth profiling 1000s (f) 1.5g/cc 3C charging 1C discharging depth profiling 1000s

Two peaks are specified in the figure 27 and 28 which showed O 1s spectrum. More other components were concealed within signs, but it is certainly difficult to distinguish the peaks. The signal of the higher binding energy of 533.8 eV was assigned to organic carbonate (RCO_3), and the peak of 532.1 eV was assigned to lithium carbonate, and the peak of 528.3 eV was assigned to lithium oxide. The oxide signal of polyethylene oxide (PEO) previously found in SEI has within the Li_2CO_3 section of O 1s. The oxide was found to have the highest intensity in the anode of 1.7g/cc discharged at 1C charged at 5C.

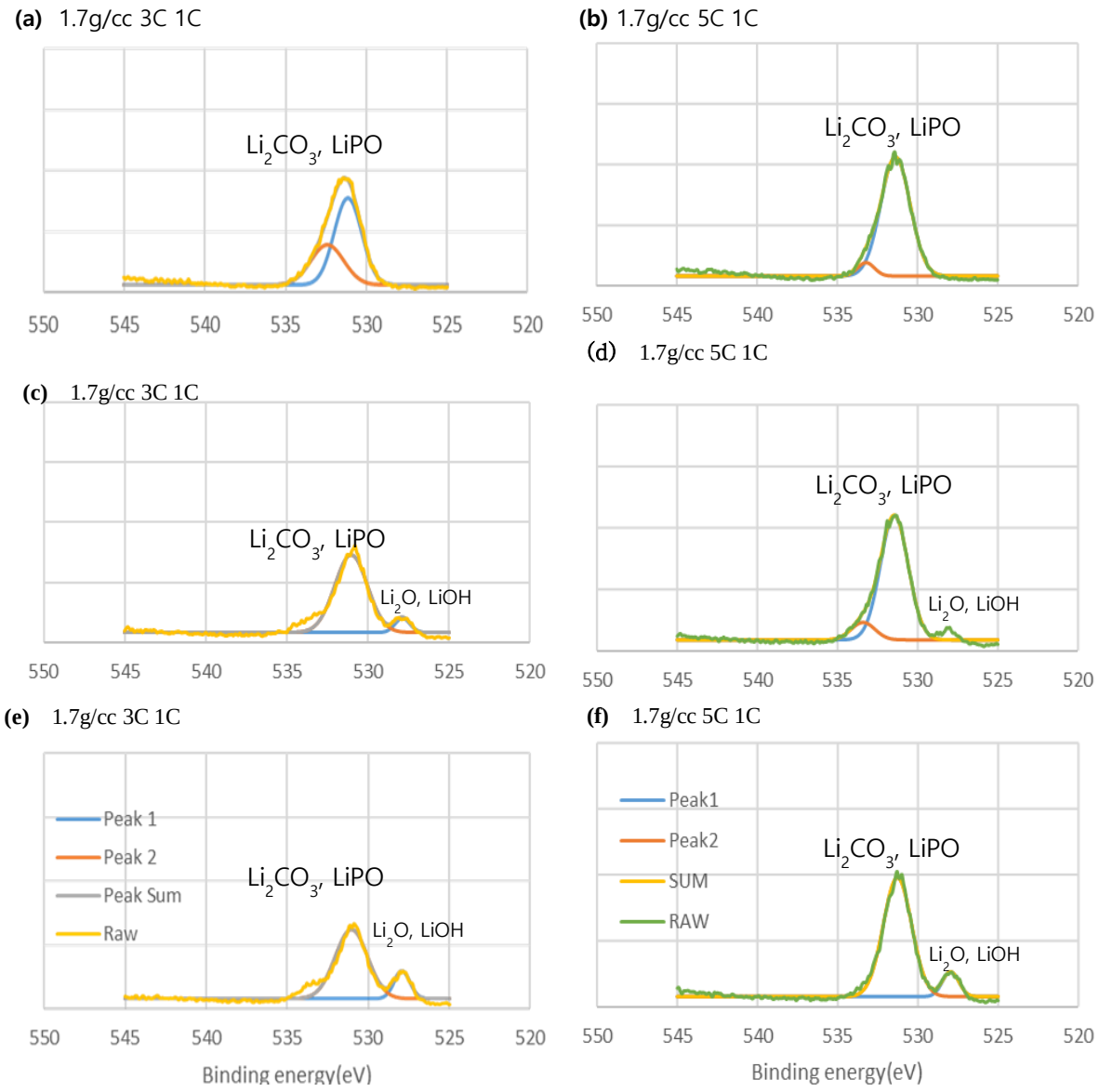

Figure 28. O 1s XPS spectra of anode (a) 1.7g/cc 3C charging 1C discharging depth profiling 0s (b) 1.7g/cc 5C charging 1C discharging (c) 1.7g/cc 3C charging 1C discharging depth profiling 200s (d) 1.7g/cc 5C charging 1C discharging depth profiling 200s (e) 1.7g/cc 3C charging 1C discharging depth profiling 1000s (f) 1.7g/cc 5C charging 1C discharging depth profiling 1000s

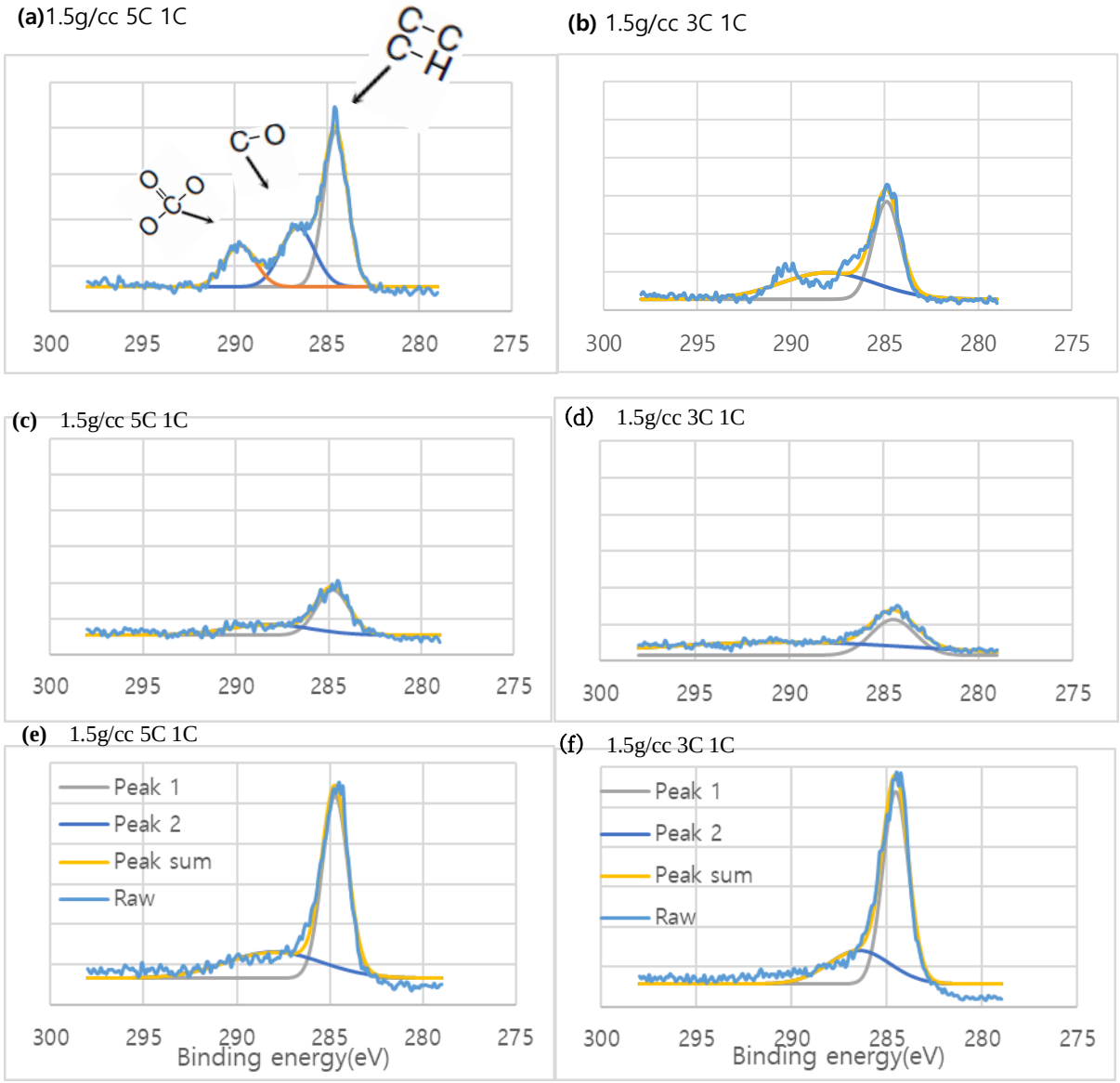

Figure 29. C 1s XPS spectra of anode (a) 1.5g/cc 5C charging 1C discharging depth profiling 0s (b) 1.5g/cc 3C charging 1C discharging (c) 1.5g/cc 5C charging 1C discharging depth profiling 200s (d) 1.5g/cc 3C charging 1C discharging depth profiling 200s (e) 1.5g/cc 5C charging 1C discharging depth profiling 1000s (f) 1.5g/cc 3C charging 1C discharging depth profiling 1000s

Figure 29 and 30 showed the XPS spectra of C 1s. Three main peaks are seen during charging. The first peak at 285.0 eV is caused by hydrocarbon impurity and carbon atoms bonded only to carbon or hydrogen atoms. The second peak is attributed to a carbon atom in only one oxygen circumstances at 286.8 eV, while the third is assigned to a carbon atom in 3 oxygen circumstances at 290.1 eV.

The binding energy point ,284.5 eV, is assigned to graphite, while the other components come from the first layer formed on the surface, mainly by cycling the electrode in fast charging. The peak at 286.8 eV may be due to a carbon atom bonded to one oxygen in lithium alkyl carbonate ($R–CH_2–OCO_2Li$). The lithium alkyl carbonate species have been labeled as the major constituents of SEI that form on anode electrodes.[19]

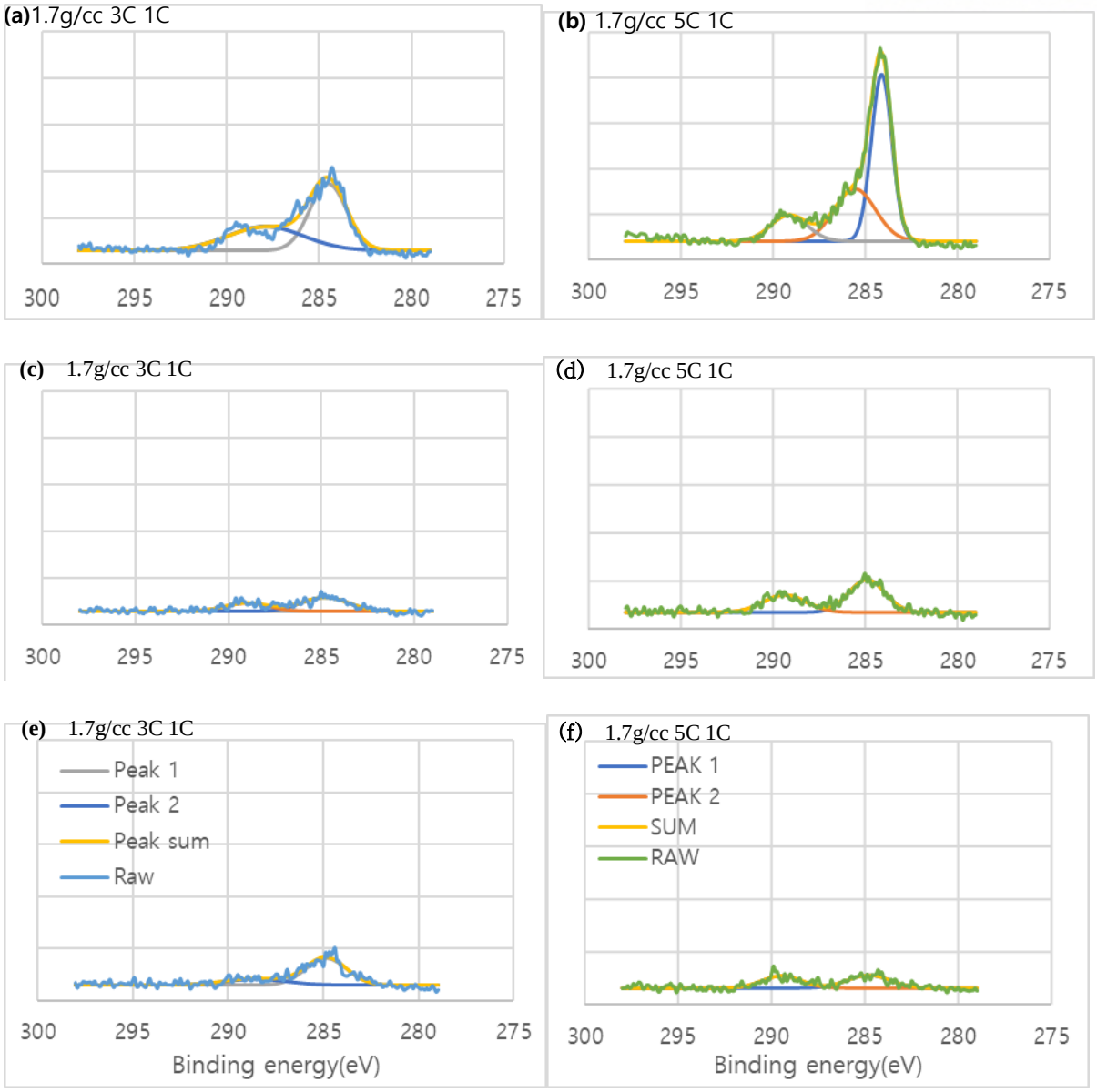

Figure 30. C 1s XPS spectra of 1.7g/cc anode (a) 1.7g/cc 3C charging 1C discharging depth profiling 0s (b) 1.7g/cc 5C charging 1C discharging (c) 1.7g/cc 3C charging 1C discharging depth profiling 200s (d) 1.7g/cc 5C charging 1C discharging depth profiling 200s (e) 1.7g/cc 3C charging 1C discharging depth profiling 1000s (f) 1.7g/cc 5C charging 1C discharging depth profiling 1000s

Ⅳ. Conclusion

The necessary to reduce range anxiety and meet customer prospects has driven many automakers to aim for rapid charging capability as a crucial design characteristic for EV battery packs

Anode electrode densities change occur ranging from 1.5g/cc to 1.7g/cc of the whole NCM811/graphite lithium-ion battery on high-rate charging. In addition, variations of charging protocol as the boost charging protocol where only a fraction of the battery capacity is charged with a high charging current, still exhibited a high drop in imbalance due to the high current boost interval.

SEM image of a 1.5g/cc graphite underwent double stage charging, taken in a charged state after 50 cycle, showed unlike other anodes with Li deposition, there is no lamination structure. On the other hand, 1.7g/cc graphite sample showed Li dendrite form taken in a charged state after 50 cycle. Therefore, 1.5g/cc graphite which underwent double stage charging not only showed good cycle life characteristics but also showed no lamination structure on the surface of graphite

In addition, surface layer growth was not even after cycling in high-rate charging and 1c discharging. LiPFx decomposes to LiF and PFx within a 1000 s sputter time; a lot of LiPFx does decompose; and by sputtering the SEI on graphite, the formation of lithiated graphite.

Reference

1. Karner, D., Garetson, T. & Francfort, J. EV Charging Infrastructure Roadmap (Idaho National Laboratory, 2016);
2. Standard J1772: Electric Vehicle and Plug in Hybrid Electric Vehicle Conductive Charge Coupler (Society of Automotive Engineers, 2017).
3. T. Waldmann, B.-I. Hogg, M. Kasper, S. Grolleau, C.G. Couceiro, K. Trad, B.P. Matadi, M. Wohlfahrt-Mehrens, Interplay of operational parameters on lithium deposition in lithium-ion cells: systematic measurements with reconstructed 3-electrode pouch full cells, J. Electrochem. Soc. 163 (2016) A1232–A1238,
4. M. Ebner, V. Wood, Tool for tortuosity estimation in lithium ion battery porous electrodes, J. Electrochem. Soc. 162 (2014) A3064–A3070,
5. Arora, Pankaj, Marc Doyle, and Ralph E. White. "Mathematical modeling of the lithium deposition overcharge reaction in lithium-ion batteries using carbon-based negative electrodes." Journal of The Electrochemical Society 146.10 (1999): 3543. J.C. Burns, D.A. Stevens, J.R. Dahn, In-situ detection of lithium plating using high precision Coulometry, J. Electrochem. Soc. 162 (2015) A959–A964,
6. J.C. Burns, D.A. Stevens, J.R. Dahn, In-situ detection of lithium plating using high precision Coulometry, J. Electrochem. Soc. 162 (2015) A959–A964,
7. D. Anseán, M. Dubarry, A. Devie, B.Y. Liaw, V.M. García, J.C. Viera, M. González, Operando lithium plating quantification and early detection of a commercial LiFePO 4 cell cycled under dynamic driving schedule, J. Power Sources 356 (2017) T. Waldmann et al. Journal of Power Sources 384 (2018) 107–124 121 36–46
8. Waldmann, Thomas, Björn-Ingo Hogg, and Margret Wohlfahrt-Mehrens. "Li plating as unwanted side reaction in commercial Li-ion cells–A review." Journal of Power Sources 384 (2018): 107-124.
9. Zhang, Rui, et al. "Conductive nanostructured scaffolds render low local current density to inhibit lithium dendrite growth." Advanced Materials 28.11 (2016): 2155-2162.
10. Brissot, C., et al. "Dendritic growth mechanisms in lithium/polymer cells." Journal of power sources 81 (1999): 925-929.
11. Sano, Hikaru, et al. "Effect of Current Density on Nucleation and Morphology of Lithium during Electrodeposition in Ionic Liquids." ECS Meeting Abstracts. No. 2. IOP Publishing, 2014.

12. C. Brissot,M. Rosso, J.-N. Chazalviel, and S. Lascaud, J. Power Sources, 81-82, 925 (1999).

13. Rosso, Michel. "Electrodeposition from a binary electrolyte: new developments and applications." Electrochimica Acta 53.1 (2007): 250-256.Pei, Allen, et al. "Nanoscale nucleation and growth of electrodeposited lithium metal." Nano letters 17.2 (2017): 1132-1139.

14. Pei, Allen, et al. "Nanoscale nucleation and growth of electrodeposited lithium metal." Nano letters 17.2 (2017): 1132-1139.

15. Tomaszewska, Anna, et al. "Lithium-ion battery fast charging: a review." ETransportation 1 (2019): 100011.

16. Guo Z, Liaw BY, Qiu X, Gao L, Zhang C. Optimal charging method for lithium ion batteries using a universal voltage protocol accommodating aging. J Power Sources 2015;274:957e64

17. Hu, Chuanyue, et al. "Synthesis and electrochemical properties of Li [Ni x Co y Mn 1− x− y] O 2 (x, y= 2/8, 3/8) cathode materials for lithium ion batteries." Rare Metals 28.1 (2009): 43-48.

18. Andersson, Anna M., et al. "Electrochemically lithiated graphite characterised by photoelectron spectroscopy." Journal of Power Sources 119 (2003): 522-527.

19. Leroy, S., et al. "Surface film formation on a graphite electrode in Li-ion batteries: AFM and XPS study." Surface and Interface Analysis: An International Journal devoted to the development and application of techniques for the analysis of surfaces, interfaces and thin films 37.10 (2005): 773-781.

20. Tsukasaki, Hirofumi, et al. "Exothermal behavior and microstructure of a LiNi1/3Mn1/3Co1/3O2 electrode layer using a Li4SnS4 solid electrolyte." Journal of Power Sources 479 (2020): 228827.

21. (J. –M. Tarascon and M.Armand: Nature 414 (2001) 359)

Acknowledgements

In particular , I would like to express my gratitude to the CNS laboratory for delivering high-quality electrolytes while working on the project “A rapid Charging Battery and its prototype cells retaining high energy density” together, and to NESM laboratory who provided high-quality single-particle NCM811 cathode materials.

Finally I am greatly grateful to my advisor professor Kyeong-Min Jeong and I wish member of ECheSL were full happiness